Chapter 1

MAGNETOHYDRODYNAMIC JETS AND WINDS FROM ACCRETION DISKS

H.C. SPRUIT

Max-Planck-Institut für Astrophysik
Postfach 1523, D-85740 Garching, Germany

Abstract

The theory of magnetically accelerated outflows and jets from accretion disks is reviewed at an introductory level, with special attention to problem areas like the launching conditions of the flow at the disk surface, stability of the magnetic field, and collimation mechanisms. This text will appear in R.A.M.J. Wijers, M.B. Davies and C.A. Tout, eds., *Physical processes in Binary Stars*, Kluwer Dordrecht, 1996 (NATO ASI series).

1.1 Introduction: the case for magnetic acceleration

Narrow, high speed outflows (jets) and less well collimated 'bipolar' outflows are observed from very different cosmical objects, ranging from protostars in the solar neighborhood, to galactic X-ray binaries, to the nuclei of active galaxies. The magnetic acceleration mechanism for outflows from accretion disks has gained significant popularity as an explanation for each of these forms of outflow. The model can account for high speeds (for example, Lorentz factors of 10 or higher in AGN and galactic black hole binaries), high degrees of collimation, and large momentum fluxes. Though other processes can also, to varying degrees, account for these properties (e.g. Blandford 1993), the magnetic model combines them in a natural way. While some processes are very different in protostellar disks and the AGN or X-ray binary disks, in particular those that produce the observed radiation, the physics of the magnetic acceleration model is to a large degree independent of these. Progress made by development of the model for explaining

observations in one area is therefore likely to have impact for the interpretation of other outflows as well.

In spite of the rather general applicability of the magnetic mechanism, it is unlikely that it is involved in all cases. There are a number of bipolar looking objects in the sky where the explanation may well be purely hydrodynamical, such as the outflows in η Carinae, and in particular the planetary nebulae (Icke et al. 1992).

The protostellar outflows play a key role in supporting the magnetic/centrifugal model. The momentum flux in these objects can be measured from flow speeds and inferred mass densities, and in many cases turns out to be much larger than can be accounted for by the nearest competing mechanism, radiation pressure from the central star (for a review see Königl and Ruden, 1993). The protostellar outflows are also the ones in which observations are most likely, in the near future, to reveal their inner workings by direct imaging, as shown in table 1.1. See the contributions elsewhere in this volume for more about this subject.

1.2 Presence of jets and outflows in binaries

Jets are now known from all classes of X-ray binaries, i.e. mass transfering binaries (Lewin et al. 1995) in which the primary is a black hole or neutron star. (Ignoring here the 'supersoft' X-ray binaries in which the primaries appear to be white dwarfs). Among the massive X-ray binaries (HMXB) in which the companion is an early type star, there are the well known jets of SS 433, and the radio jets from Cyg X-3 (Strom, van Paradijs and van der Klis, 1989) and the galactic center source 1E140.7 - 2942 (Mirabel et al. 1992). Among the low mass X-ray binaries (LMXB) with neutron star primaries, a jet is known only from Cir X-1 (Stewart et al. 1993). Until recently no jets were known from LMXB with black hole candidate primaries, but this has changed with the discovery of superluminal jets in the variable source GRS 1915+105 (Mirabel 1994), and the transient GRO 1655-40 (= X-ray Nova Sco 1994), (Hjellming and Rupen 1995). The physics in the inner disks of these objects must be rather similar to that in the central engines of AGN (e.g. Begelman, Blandford and Rees 1984), and it is pleasing to see that they can produce very similar jets, though on a much smaller scale (for more observational similarities between galactic black hole candidates and AGN see Sunyaev et al. 1991 and references therein).

Outflows without evidence for jets exist in Cataclysmic Variables (CV: binaries

Table 1.1: Angular size of the accelerating region (assumed to be 100 times the typical size r_0 of the inner disk) for jet-producing objects.

	inner disk r_0	distance D	angular scale (") $100\,r_0/D$
nearby protostar	$3R_\odot$	500 pc	0.003
nearby active galactic nucleus	100 AU	10 Mpc	0.001
galactic black hole candidate	100 km	2 kpc	$3\,10^{-8}$

transfering mass from a main sequence star to a white dwarf, see Hack and La Dous, 1993). P-Cygni profiles indicating mass loss are seen in UV lines in Dwarf Novae (DN) when in outburst (e.g. Drew and Verbunt, 1988). No evidence for outflow is known for DN in quiescence. In UX Uma systems (CV with steady mass transfer), evidence for mass loss comes from single-peaked line profiles (in contrast with the classical double-peaked profiles of accretion disks), and the presence of additional 'uneclipsed light' in eclipsing systems ('SW Sex syndrome', Thorstensen et al. 1991). It is fair to say that no collimated outflow has yet been observed from a CV. One might wonder if this has something to do with the fact that the primaries are white dwarfs, but the case of R Aqr shows that this cannot be the case. R Aqr is a white dwarf with a Mira type giant companion in a 44 yr orbit; mass transfer occurs because of the dense stellar wind from the Mira. It has a jet which is visible at optical as well as radio wavelengths (Burgarella and Paresce 1992, Dougherty et al. 1995).

It is still somewhat puzzling that among the bright LMXB containing neutron stars there is only one case with a jet (Cir X-1). Also, it is not clear why jets have been found only in a few of the relatively frequent (1-2 yr^{-1}) bright X-ray transients. These systems are believed to be all rather similar. This indicates that there may be additional factors determining the production of jets, factors for which no observational counterparts have been identified so far.

Protostellar binaries are a bit of a different class of objects in this context, since their disks are not fed by mass transfer. The effects of a binary companion on a protostellar disk, however, may well be relevant for the ability of the object to produce a jet. I return to this question in the last section.

1.3 Physics of magnetic acceleration: heuristics

Magnetized winds and jets can be produced by rotating objects which, for one reason or the other, have a magnetic field anchored in them. The importance of such a magnetic field for the spindown of stars was realized by Schatzman (1962) soon after the discovery of the solar wind. Quantitative models for magnetized stellar winds were then developed by Weber and Davis (1967) and Mestel (1968). The point of view in this work was, mostly, the spindown of stars, but Michel (1969, 1973, see also Goldreich and Julian 1970) realized the importance of the mechanism for producing high speed outflows, and formulated relativistic models for magnetic winds from pulsars. That strong outflows could also be driven magnetically by accretion disks was proposed by Bisnovatyi-Kogan and Ruzmaikin (1976), Blandford (1976) and Lovelace (1976). Workable quantitative models for such flows were first produced by Blandford and Payne (1982), while full numerical solutions for the steady (nonrelativistic) problem were first obtained by Sakurai (1985, 1987).

In this section I review, at a heuristic level, the basic ideas and processes involved. The theory is introduced a bit more formally in the next section. For definiteness a wind generated by an accretion disk is considered here. Most of the discussion however, applies equally well to rotating stars.

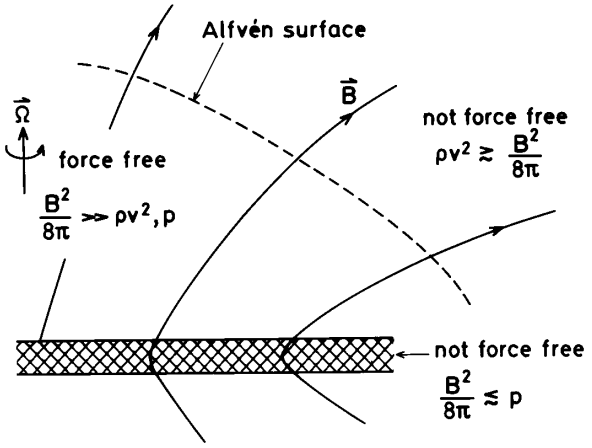

Figure 1.1: Regions of force-free and non-force free magnetic field in a disk-driven wind.

First, divide the disk and its surrounding space according to the relative importance of the magnetic field energy density, see fig. 1.1. The magnetic field to be used for producing the wind is anchored in the disk, so its energy density there must be less than the rotational kinetic energy in the disk. It can exceed the thermal energy density in principle, but in any case its strength and configuration is determined by other forces, which provide the anchoring of the field. Just how large the field strength is, for any kind of observed disk, is still unknown since no field strengths have been measured yet[1]. Theoretical arguments allow for field strengths of the order of equipartition with the gas pressure, in the case of dynamo-generated fields (e.g. Hawley et al. 1995, Brandenburg et al. 1995), or even larger field strengths for magnetic flux dragged in with the accretion flow (Spruit, Stehle and Papaloizou 1995, Lubow and Spruit 1995). Without being too specific, I assume that the vertical field strength, at the disk surface, is reasonably large, since the magnetic acceleration mechanism requires a field of some strength (a more specific criterion is given in sect. 1.7). Outside the disk, the gas density is typically so low (assuming a cool disk) that the magnetic energy density is large compared with the thermal and rotational energies. The field in this region must therefore be *force free*, much like the solar corona (e.g. Foukal 1990). In the absence of torques acting on it, it must even be a *potential field*. As fig. 1.1 suggests, we are assuming that the field is of uniform polarity, over the region of the disk where the wind is generated. Loops of field connecting different parts of the disk cannot be excluded a priori. Such loops are sheared rapidly by differential rotation, giving rise to a rich and not very well understood complex of phenomena which is outside the scope of this discussion. It suffices that a certain minimal

[1] An exception is the field strength (about 1 G) in the protosolar nebula inferred from meteorites (e.g. Cisowski and Hood 1991)

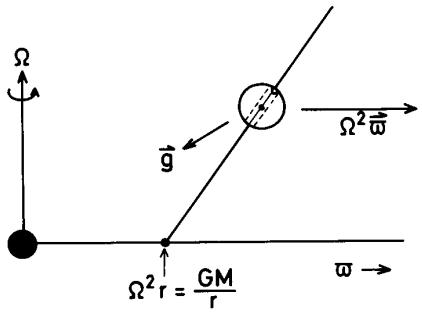

Figure 1.2: Bead-on-a-wire analogy for centrifugal acceleration by a magnetic field.

fraction of the disk's magnetic flux does not loop back to the disk surface, but is open to infinity.

As the flow is accelerated, the field strength drops due to the increasing distance from the disk. The acceleration effectively stops when the flow speed reaches the local Alfvén speed in the flow. The place where this happens is called the Alfvén surface. Thus, outside the region where the magnetic field dominates there is again a region where the field is not force free; in this case because of inertial forces (fig. 1.1).

The acceleration process is illustrated in fig. 1.2. Assume that the disk is cool, so that its rotation is close to Keplerian, and its thickness can be neglected. Also assume that the gas is sufficiently ionized everywhere that ideal MHD can be used, i.e. that gas is tied to the field lines. These assumptions are not essential and can be relaxed in numerical models, such as those of Königl (1989). Assuming we are close to the disk surface, and the field strength large, the atmosphere of the disk is forced to corotate with the field lines sticking out of the surface. Since the Lorentz force only has components perpendicular to the field, the gas is free to move along the field line, under the influence of the other forces, like a 'bead on a wire'. At the foot point of the field line, the inward force of gravity just balances the centrifugal force, because of our assumption of Keplerian rotation in the disk. Along the field line, the centrifugal force increases with distance from the axis. When the component of the centrifugal force along the field line exceeds that of gravity, the gas tied to the field line is accelerated outward.

This centrifugal process stops when the flow speed becomes comparable to the Alfvén speed; at that point, the field is no longer strong enough to enforce corotation.

Depending on one's preferences, the acceleration can also be described in purely magnetic terminology (e.g. Lovelace, Wang and Sulkanen 1987), without appealing to a centrifugal force. This is discussed in sect. 1.4.1.

Beyond the Alfvén surface, the inertia of the gas causes it to lag behind the rotation of the field line, so that the field gets wound up. The simplest way to visualize this is by ignoring the rotation of the gas altogether. Then for each

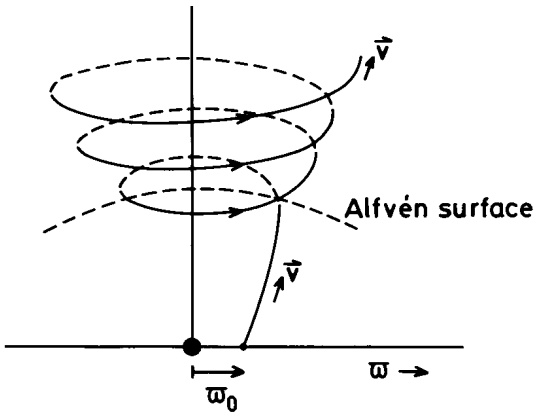

Figure 1.3: Development of the azimuthal field. With each rotation of the field line a loop of field is added to the flow at the Alfvén surface.

rotation of the foot point of the field line, one loop of field is added at the Alfvén surface. As the flow carries these loops away, a spiral shaped field formed (fig. 1.3) with pitch v/Ω, where v is the flow speed and Ω the rotation rate of the foot point. In a (nonrotating) frame comoving with the flow, one sees a nearly azimuthal magnetic field, its strength decreasing with time. The curvature force in the azimuthal field is directed towards the axis, causing the flow to 'collimate', i.e. to become parallel to the rotation axis.

A numerical example of a magnetically accelerated flow is shown in fig. 1.4. Note that the rotation velocity peaks near the Alfvén radius $r_{\rm A}$, which is at 100 times the starting distance r_0 in this example. At large distance, the rotation drops roughly in accordance with angular momentum conservation. The asymptotic radial velocity is larger than the rotation speed at $r_{\rm A}$ by a factor of order unity.

One of the attractions of the magnetic wind model is that it not only produces outflow, but in principle can also take out the angular momentum from the disk, allowing it to accrete (Blandford 1976, Bisnovatyi-Kogan and Ruzmaikin 1976). To see how effective this can be let us estimate the angular momentum flux carried by the wind. Since the flow corotates roughly up to the Alfvén point, the specific angular momentum carried is of the order $\Omega r_{\rm A}^2$, hence

$$\dot{J}_{\rm w} = \dot{M}_{\rm w}\Omega r_{\rm A}^2, \tag{1.1}$$

where $\dot{M}_{\rm w}$ is the mass flux on a field line with foot point r_0. It turns out that this estimate is actually exact (sect. 1.4). The angular momentum that has to be extracted (locally at r_0) from a Keplerian disk in order for it to accrete at a rate $\dot{M}_{\rm a}$ is $\dot{J}_{\rm a} = \frac{1}{2}\Omega r_0^2\dot{M}_{\rm a}$, hence

$$\frac{\dot{M}_{\rm w}}{\dot{M}_{\rm a}} = \frac{1}{2}\left(\frac{r_0}{r_{\rm A}}\right)^2. \tag{1.2}$$

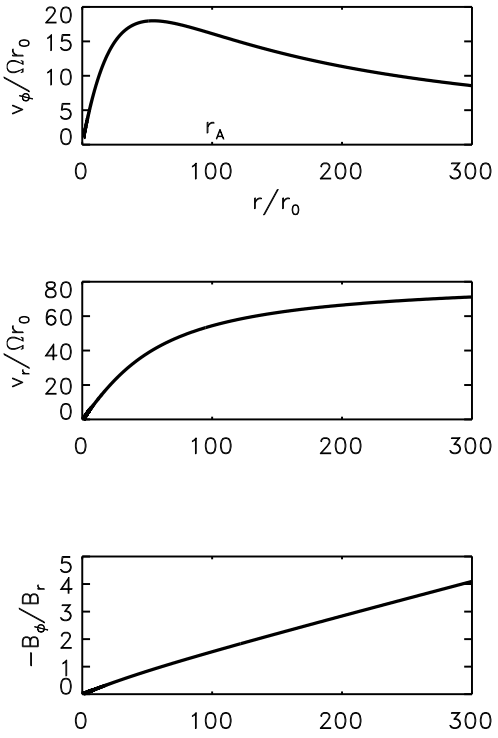

Figure 1.4: Example of a magnetic wind model. Top 2 panels: rotation velocity (measured in an inertial frame) and radial velocity in units of the rotation speed at the base of the flow, as functions of distance. Alfvén radius is at $100r_0$. Lower panel: field angle. (Cold WD model for $\mu = 10^{-6}$, see text).

Since this relation is exact, and r_A always larger than r_0, it follows that only a fraction of the mass flux in the disk can flow out in the wind. It is possible in principle, however, that the wind carries away all angular momentum that the disk has to loose in order to accrete, i.e. without angular momentum transport by viscous torques in the disk. Such a disk would, in the absence of viscous dissipation, be silent. This is verified by looking at the energy balance. The energy flux $\dot{E}_\mathrm{w}$ in the wind is given by $\Omega \dot{J}_\mathrm{w}$ (the work done against the wind torque). If all the angular momentum is carried with the wind we have $\dot{E}_\mathrm{w} = \dot{E}_\mathrm{a}$ (using eq. 1.2), where $\dot{E}_\mathrm{a} = 1/2(\Omega r_0)^2 \dot{M}_\mathrm{a}$ is the rate of gravitational energy release in a Keplerian disk. Thus, if the wind carries away all the angular momentum, it also carries away all the accretion energy.

1.3.1 Structure of a disk driven wind

The magnetically driven wind is conveniently broken down into three conceptual stages or subprocesses. Near the disk surface, the wind is 'launched': details

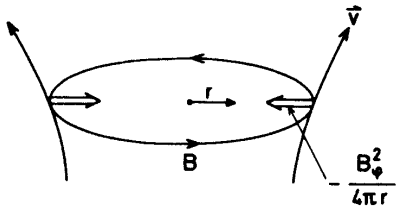

Figure 1.5: Collimation of the flow by the curvature force of the azimuthal magnetic field.

of disk structure and magnetic field configuration near this surface determine how much mass is launched into a flow. After this, the flow can be regarded as ballistic, its acceleration being governed almost entirely by gravitational and magnetic/centrifugal forces. After the acceleration phase, which ends roughly at Alfvén surface, the collimation phase starts, in which the flow is deflected towards the axis by 'hoop stress' (fig. 1.5).

Since the outer radius of a disk is typically much larger than the inner radius, conditions can vary dramatically with distance in the disk. The wind problem is, therefore, a function of distance. In the inner regions where the field strength and the rotation speed are large, conditions are favorable for producing high speed collimated winds. In the outer regions, one would expect lower wind speeds, and probably less collimation. The fluxes of mass and angular momentum from the outer regions, on the other hand, could be large compared to flows from the inner regions. Flows from these regions may well coexist. Since the magnetic field inside the Alfvén radius is force free, its configuration is determined by a global force balance. The wind properties from adjacent regions in the disk are therefore coupled somewhat, through their dependence on the shape of the poloidal field. This aspect of the disk wind problem has not yet received much attention.

In the next sections this picture is elaborated a bit more formally. In the process, some problem areas of current interest will be noted, relating, in particular, to the launching and collimation phases.

1.4 Steady axisymmetric magnetic flows

The theory of magnetically driven flows from rotating objects has been given in many texts (e.g. Weber and Davis 1967, Mestel 1968, Heinemann and Olbert 1978, Okamoto 1975, Blandford and Payne 1982). I repeat the basic derivation here, under the assumption of ideal magnetohydrodynamics, in the nonrelativistic limit. The extension to relativistic MHD can be found in Michel (1969), Goldreich and Julian (1970), Bekenstein and Oron (1978), Camenzind (1987), for a general treatment of relativistic MHD see Lichnérowicz (1967).

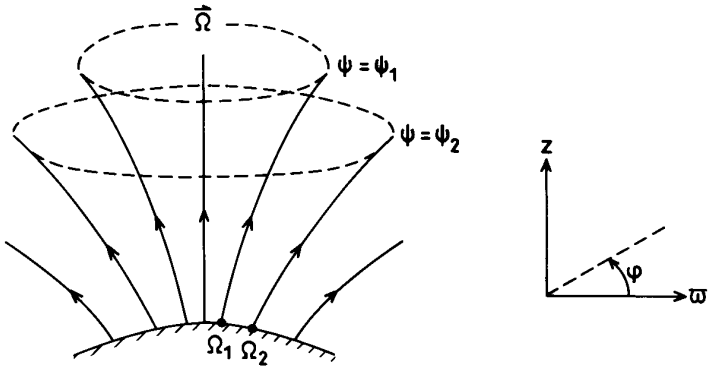

Figure 1.6: Axisymmetric poloidal magnetic anchored in a rotating object. Magnetic surfaces are labeled by the flux function ψ. Rotation rate can be a function of ψ.

The basic assumptions made are the MHD approximation, and that the flow is stationary and axisymmetry. The MHD approximation is justified if the rotating object actually produces an outflow of any observational significance; it holds if the density of charge carriers is large compared with the so-called Goldreich-Julian density, $N_{GJ} = \Omega B/(4\pi ce) \sim 10^{-2}\Omega B$ cm^{-3}. This limit is of importance in the case of pulsar magnetospheres (Goldreich and Julian 1969), but is so low that it is not likely to become relevant for most of the observable winds and jets. Though deviations from stationarity are implied by the production of outward traveling 'knots' in most jets (for an example see Mirabel and Rodriguez 1994), the time scale for acceleration is still likely to be short compared to the time scale of these variations, so that stationarity is a good assumption during the acceleration phase. Much of the jet phenomenology is consistent with axisymmetry. Theoretically, nonaxisymmetric instabilities are likely to become important in parts of the jet; this is discussed further below. Keeping this in mind, we proceed with the axisymmetric case. The final assumption made is that of infinite conductivity. This can easily be relaxed (Königl 1989), but deviations from this approximation are important only in the case of protostellar jets, where the flows are so cool that the conductivity needs to be considered in detail.

The equations for stationary ideal MHD are (e.g. Roberts, 1967)

$$\nabla \times (\mathbf{v} \times \mathbf{B}) = 0, \tag{1.3}$$

$$\rho \mathbf{v} \cdot \nabla \mathbf{v} = -\nabla p - \rho \nabla \Phi + \frac{1}{4\pi}(\nabla \times \mathbf{B}) \times \mathbf{B}, \tag{1.4}$$

$$\nabla \cdot (\rho \mathbf{v}) = 0, \tag{1.5}$$

$$\nabla \cdot \mathbf{B} = 0. \tag{1.6}$$

Here $\mathbf{B}, \mathbf{v}, \Phi, p, \rho$ are the magnetic field vector, the velocity, the gravitational potential, the gas pressure and the density. Using cylindrical coordinates (ϖ, ϕ, z),

axisymmetric vectors like $\mathbf{B}$ and $\mathbf{v}$ can be written in terms of their poloidal ($_\mathrm{p}$) and toroidal ($_\phi$) components:

$$\mathbf{B} = \mathbf{B}_\mathrm{p} + B_\phi \mathbf{e}_\phi, \qquad \mathbf{v} = \mathbf{v}_\mathrm{p} + v_\phi \mathbf{e}_\phi, \tag{1.7}$$

where the poloidal components lie in the meridional (ϖ, z) plane.

With the assumed axisymmetry, these equations have a great deal of symmetry, so that they can, in part, be reduced to algebraic equations. This is done as follows. Due to axysimmetry and div$\mathbf{B} = 0$, $\mathbf{B}_\mathrm{p}$ can be written in terms of a *flux function* ψ:

$$\mathbf{B}_\mathrm{p} = \frac{1}{\varpi} \nabla\psi \times \mathbf{e}_\phi, \tag{1.8}$$

i.e. $B_z = 1/\varpi\, \partial\psi/\partial\varpi$, $B_r = -1/\varpi\, \partial\psi/\partial z$. The flux function (also called stream function or vector potential) is constant along field lines:

$$\mathbf{B} \cdot \nabla\psi = 0. \tag{1.9}$$

Thus, ψ can be read as a *label* numbering the field lines of the poloidal field (fig. 1.6). It plays an important role in this numbering capacity, since there will be several scalar fields α with the property $\mathbf{B}_\mathrm{p} \cdot \nabla\alpha = 0$. Such fields have their gradients parallel to that of ψ, and therefore are functions of ψ only, and are also constant on field lines. From (eq. 1.3) we have $\mathbf{B} \times \mathbf{v} = \nabla f$, where f is an axisymmetric scalar. Writing this out into poloidal and toroidal components:

$$\mathbf{v}_\mathrm{p} \times \mathbf{B}_\mathrm{p} + v_\phi \mathbf{e}_\phi \times \mathbf{B}_\mathrm{p} + B_\phi \mathbf{v}_\mathrm{p} \times \mathbf{e}_\phi = \nabla f. \tag{1.10}$$

The toroidal component of this is

$$\mathbf{v}_\mathrm{p} \times \mathbf{B}_\mathrm{p} = 0, \qquad \text{or} \qquad \mathbf{v}_\mathrm{p} = \kappa(\varpi, z)\mathbf{B}_\mathrm{p}. \tag{1.11}$$

Thus, the poloidal velocity is parallel to the poloidal magnetic field, a consequence of the infinite conductivity assumed. With (1.11), the dot product of (1.10) with $\mathbf{B}_\mathrm{p}$ yields $\mathbf{B}_\mathrm{p} \cdot \nabla f = 0$, so that f is not just a scalar, but a function of the field line number ψ only. With this, (1.10) yields

$$v_\phi - \kappa B_\phi = \varpi f'(\psi), \tag{1.12}$$

where $f' = \mathrm{d}f/\mathrm{d}\psi$. With (1.11), (1.6), the continuity equation (1.5) yields $\mathbf{B}_\mathrm{p} \cdot \nabla(\rho\kappa) = 0$, so that

$$\rho v_\mathrm{p}/B_\mathrm{p} = \rho\kappa = \eta(\psi), \tag{1.13}$$

for some function η. This equation simply states that the mass flux density, per unit of poloidal magnetic flux, is constant along a field line: each field line has its own mass flux, in this sense.

Now find the point along a poloidal field line inside the rotating object, on which $B_\phi = 0$, and call this the 'foot point' of the field line. If the object, together

with $\mathbf{B}_\mathrm{p}$, is symmetric about the equator, this point is on the equatorial plane[2]. Let $\Omega = v_{\phi 0}/\varpi_0$ be the rotation rate of this foot point. Then we find from (1.12) that $f'(\psi) = \Omega$. Loosely, we can call this the 'rotation rate of the field line'. Remember, however, that the plasma rotation rate, $\Omega_\mathrm{p} = v_\phi/\varpi$, is *not* constant along a field line. It cannot be, because the plasma corotates with the foot point only as long as the field is strong enough to dominate over the plasma; the rotation starts lagging behind at larger distances from the object where the field is weaker. Let $\mathbf{v}'$ be the flow velocity measured in a frame rotating with the angular frequency Ω:

$$\mathbf{v}' = \mathbf{v} - \varpi\Omega(\psi)\mathbf{e}_\phi \tag{1.14}$$

Then (1.12) and (1.11) can be combined into

$$\mathbf{v}' = \kappa\mathbf{B}. \tag{1.15}$$

In other words, in a frame corotating with the foot point of a field line, the flow is everywhere parallel to the magnetic field (this frame can be different for each poloidal field line, if the object rotates differentially). Whereas the *poloidal* flow component is parallel to the *poloidal* field component in both the rotating and the stationary frames, the total velocity is parallel to the total B-field only in a corotating frame.

Next, consider the equation of motion (in a non-rotating frame). Using axisymmetry and the identity $(\nabla \times \mathbf{B}) \times \mathbf{B} = -\nabla B^2/2 + (\mathbf{B}\cdot\nabla)\mathbf{B}$, the toroidal component is

$$\rho(\mathbf{v}\cdot\nabla\mathbf{v})_\phi = \frac{1}{4\pi}(\mathbf{B}\cdot\nabla\mathbf{B})_\phi. \tag{1.16}$$

With the vector relation $(\mathbf{a}\cdot\nabla\mathbf{b})_\phi = \mathbf{a}\cdot\nabla(\varpi b_\phi)/\varpi$, (1.11) and (1.13), this can be written as

$$\mathbf{B}_\mathrm{p}\cdot\nabla(\rho\kappa\varpi v_\phi) = \frac{1}{4\pi}\mathbf{B}_\mathrm{p}\cdot\nabla(\varpi B_\phi). \tag{1.17}$$

This can be integrated, yielding

$$\frac{1}{B_\mathrm{p}}(\rho v_\mathrm{p}\varpi v_\phi - \frac{\varpi}{4\pi}B_\phi B_\mathrm{p}) = \eta L, \tag{1.18}$$

where L is a a function of ψ only. Hence

$$\varpi(v_\phi - \frac{1}{4\pi\eta}B_\phi) = L(\psi). \tag{1.19}$$

The first term in (1.18) is the flux of angular momentum by the poloidal flow, the second the magnetic torque. Thus, (1.18) expresses that the total flux of angular momentum, per unit of poloidal magnetic flux, is constant along each field line.

[2] Such symmetry simplifies the visualization, but is not necessary. All poloidal field lines are 'bent back' at the object's surface by the wind torque in the same direction (lagging behind the rotation), so that B_ϕ is of opposite signs at two successive crossings of the field line through the object's surface. Hence on all poloidal field lines crossing the surface the toroidal component changes sign at some point inside the object.

The total angular momentum flux measured per unit of *mass* flowing along the field line is L.

Before proceeding with the equation of motion, we use (1.12) to eliminate B_ϕ from (1.19). This yields

$$v_\phi - \Omega\varpi = \frac{L - \Omega\varpi^2}{\varpi[1 - 1/(4\pi\kappa^2\rho)]}. \tag{1.20}$$

The denominator on the RHS vanishes when $4\pi\rho v_{\rm p}^2/B_{\rm p}^2 = 1$, or $v_{\rm p} = v_{\rm Ap}$, where $v_{\rm Ap} = B_{\rm p}/(4\pi\rho)^{1/2}$ is the poloidal Alfvén speed. The location along the field line where this happens is called the *Alfvén point*, because an axisymmetric Alfvén wave propagates along a magnetic surface at the speed $v_{\rm Ap}$ (independent of the value of B_ϕ). If the flow is to be accelerated to values beyond the local poloidal Alfvén speed, the numerator in (1.20) also has to vanish at the Alfvén point. If we denote the physical variables at the Alfvén point with a subscript $_{\rm A}$, this condition yields

$$L = \Omega\varpi_{\rm A}^2. \tag{1.21}$$

The interpretation of the singularity at $\varpi_{\rm A}$ is similar to that of the sonic point in the transition from subsonic to supersonic flow in ordinary hydrodynamics (jet nozzle, stellar winds). Eq. (1.21) has an important physical interpretation.

Eq. (1.21) has an important physical interpretation. If the flow were to corotate with the field up to $\varpi_{\rm A}$ (which actually it does not, see above) it would, at that point, have the specific angular momentum given by (1.21). Since L is the specific angular momentum flux in the wind (including the magnetic torque!), it is as if the flow were kept rigidly corotating out to $\varpi_{\rm A}$, and then released without further magnetic torques. As far as the angular momentum flux is concerned, the flow 'effectively corotates' out to ϖ_A.

As in ordinary dissipationless hydrodynamics, the equation of motion in the direction of the flow can be integrated in terms of a Bernoulli function, provided that the energy equation is sufficiently 'simple'. In practice this is the case if polytropic or isothermal equations of state can be used as approximations:

$$P = K\rho^\gamma, \tag{1.22}$$

where K, γ are constants. The isothermal case is obtained with $\gamma = 1$. These are not necessarily very good approximations to the real situation, since energy dissipation and cooling processes usually are present. These play an important role in the early stages of the acceleration, see sect. 1.5.3. Once the flow has been accelerated beyond the speed of sound, however, the dynamics does not depend much on the temperature of the gas any more.

In a corotating frame (corotating with the foot point of the field line, cf. the discussion above), the equation of motion becomes:

$$\rho\mathbf{v}' \cdot \nabla\mathbf{v}' = -\nabla p + \frac{1}{4\pi}(\nabla \times \mathbf{B}) \times \mathbf{B} - \rho\nabla\Phi + \rho\Omega^2\boldsymbol{\varpi} + 2\rho\mathbf{v}' \times \boldsymbol{\Omega}, \tag{1.23}$$

where $\boldsymbol{\varpi} = \varpi\mathbf{e}_\phi$ and Φ is the gravitational potential:

$$\Phi = -\frac{GM}{r}. \tag{1.24}$$

Let **s** be a unit vector parallel to the magnetic field. Taking the dot product of (1.23) with **s**, we get the component of the equation of motion parallel to the field lines. I denote the derivative along the field line by

$$\partial_s \equiv \mathbf{s} \cdot \nabla. \tag{1.25}$$

Then the centrifugal term $\Omega^2 \mathbf{s} \cdot \boldsymbol{\varpi}$ can be written as $\partial_s(\Omega^2 \varpi^2/2)$, since Ω is a constant along a field line (remember it is the foot point rotation rate, not the local fluid rotation). The Coriolis term disappears because it is perpendicular to **v**, which is parallel to **B** in the rotating frame. The magnetic term disappears because the Lorentz force is perpendicular to **B**. Thus (1.23) yields

$$\partial_s \frac{1}{2} v'^2 = -\frac{1}{\rho}\partial_s p - \partial_s \Phi + \partial_s(\frac{1}{2}\Omega^2 \varpi^2). \tag{1.26}$$

With the polytropic equation of state, the thermal term can be written as

$$\frac{1}{\rho}\partial_s p = \partial_s(k c_{\rm s}^2), \tag{1.27}$$

where k is a factor of order unity:

$$\begin{aligned} k &= \frac{\gamma}{\gamma - 1} \qquad (\gamma \neq 1), \\ &= \ln(\rho) \qquad (\gamma = 1), \end{aligned} \tag{1.28}$$

and

$$c_s = (p/\rho)^{1/2} \tag{1.29}$$

is the isothermal sound speed. The equation can now be integrated; with the definition v', this yields:

$$\frac{1}{2} v_{\rm p}^2 + \frac{1}{2}(v_\phi - \Omega\varpi)^2 + k c_{\rm s}^2 + \Phi - \frac{1}{2}\Omega^2 \varpi^2 = E(\psi), \tag{1.30}$$

alternatively:

$$\frac{1}{2} v^2 - v_\phi \Omega \varpi + k c_{\rm s}^2 + \Phi = E(\psi). \tag{1.31}$$

The integration constant E depends on the field line label ψ only. This is called the *Bernoulli equation*. It states that, in the rotating frame, the sum of kinetic, thermal, gravitational and a 'centrifugal energy' is constant along a field line. A look at the terms in this equation shows the basics of centrifugal acceleration. Assume that the field is strong enough to enforce approximate corotation, so that $v_\phi \approx \Omega\varpi$. Assume that we are looking at a flow which has already been accelerated to supersonic speeds, $v_{\rm p} \gg c$, so that the thermal term can be ignored compared with the first term. The kinetic energy $\frac{1}{2} v_{\rm p}^2$ then increases with distance ϖ from the axis due to the rapid decrease of the centrifugal term. This is offset by the increase of the gravitational potential Φ, but eventually the centrifugal term dominates because Φ reaches a constant value at infinity. More precisely, the condition for

outward acceleration, at any point on the field line, and still ignoring thermal effects, is:

$$\partial_s(\Phi - \frac{1}{2}\Omega^2\varpi^2) < 0 \qquad (T = 0), \tag{1.32}$$

where the arc length s is taken to increase in the direction of ϖ. The thermal term adds to the acceleration: as the flow expands outward, thermal energy is converted into kinetic energy, in the same way as in a jet nozzle. In slowly rotating stars, this is the dominant process driving the stellar wind, and one has a *thermally driven* wind (Parker 1963, for an introduction see Foukal 1990). In more rapidly rotating stars, and in our case of jets produced by disks, the thermal energy plays a role only in the initial stages, and most of the actual acceleration is centrifugal. The conditions for launching a wind from a disk are discussed further in sect. 1.5.3.

1.4.1 Acceleration: centrifugal or magnetic?

This discussion above suggests that the centrifugal force could accelerate the flow indefinitely, but this is an artefact of our assumption of corotation. When the field becomes weak with distance, the azimuthal velocity starts lagging behind $\Omega\varpi$, and then becomes small compared with $\Omega\varpi$. The second term in eq. 1.30 then nearly cancels the centrifugal term. How much acceleration still remains depends on the details of how fast v_ϕ decreases, and the other equations have to be used as well to determine this.

By working in the rotating frame there is no contribution from magnetic forces. This may seem strange, since it is ultimately the magnetic forces that transmit the rotational energy of the object in which they are anchored to the flow. That the acceleration can also be regarded as magnetic is seen by considering the equation of motion in an inertial frame. We want to know how the poloidal velocity is accelerated by the magnetic field. The poloidal component of the Lorentz force is

$$\mathbf{F}_{\rm p} = \frac{1}{4\pi}[(\nabla\times\mathbf{B})\times\mathbf{B}]_{\rm p} = \frac{1}{4\pi}[(\nabla\times\mathbf{B})_{\rm p}\times\mathbf{B}_\phi + (\nabla\times\mathbf{B})_\phi\times\mathbf{B}_{\rm p}], \tag{1.33}$$

where $_{\rm p}$ and $_\phi$ are the poloidal and toroidal components of vectors, as defined above. The second term is perpendicular to $\mathbf{B}_{\rm p}$ and $\mathbf{v}_{\rm p}$, so does not contribute to acceleration. Thus the accelerating force is the first term on the right in (1.33), which can be written as

$$\frac{1}{4\pi}(\nabla\times\mathbf{B}_\phi)\times\mathbf{B}_\phi. \tag{1.34}$$

The condition that the poloidal flow is accelerated is then $\mathbf{v}_{\rm p}\cdot(\nabla\times\mathbf{B}_\phi)\times\mathbf{B}_\phi > 0$. With (1.7) this can be written as:

$$-\mathbf{v}_{\rm p}\cdot[\nabla\frac{B_\phi^2}{8\pi} + \frac{B_\phi^2}{4\pi}\mathbf{e}_\varpi] > 0. \tag{1.35}$$

This shows that it is the pressure gradient (first term) and tension force (second term) of the *toroidal* field which determine the acceleration. For a net outward acceleration to occur, B_ϕ^2 has to decrease outward along the field line sufficiently rapidly to overcome the tension force, which is directed towards the axis. Whether

this is actually the case can not be determined from this argument, since one has to solve the full problem to find B_ϕ.

We have derived both acceleration conditions (1.32) and (1.35) from the same equation of motion, hence the *magnetic* and *centrifugal* points of view are equivalent. This can be verified by deriving the Bernoulli equation in an inertial frame. The component of the equation of motion parallel to $\mathbf{v}$ then has a magnetic term $\mathbf{v}\cdot(\nabla\times\mathbf{B})\times\mathbf{B}/(4\pi)$ instead of the centrifugal term. Using (1.13), (1.11), (1.18), the magnetic fields in this term can be replaced by velocities. The end result is eq. 1.31.

The situation at hand determines which of these views is more appropriate. In regions where the field is strong enough to enforce approximate corotation, the centrifugal view is appropriate. When corotation is not a good approximation, the acceleration is more conveniently viewed as due to the magnetic pressure of the azimuthal field. Corotation is usually a good approximation up to the Alfvén radius (with a significant exception, see sect. 1.7 below). Beyond the Alfvén radius, the field lines stop corotating, and instead are rapidly wound up into a nearly toroidal field. Here, some residual acceleration by the gradient of B_ϕ^2 takes place.

1.5 Acceleration in a fixed poloidal field

To the extent that the field above the disk can be approximated by a potential field, it depends only on the distribution of its 'sources' on the disk, namely the normal field component $B_z(\varpi, z=0)$. The accelerating flow and the toroidal field which develops in it, however, exert forces which distort the poloidal field. A full solution of the problem therefore requires solving the equation of motion in the direction perperdicular to the poloidal field lines, the 'cross-field' equation. This is considered below (section 1.6). A convenient approximation for the wind problem, however, is to consider the *poloidal* field as fixed and given. The toroidal field (which is responsible for the acceleration), is left free, to be solved for. This approximation is good for dealing with the launching and acceleration aspects of the problem in the case when the Alfvén radius is at a large distance, since most of the acceleration then takes place in the magnetically dominated region. It obviously breaks down whereever the toroidal field dominates over the poloidal component. Thus collimation of the flow by the 'hoop stress' of B_ϕ cannot be dealt with in this approximation. It also fails, in the entire domain, in the high-mass loss regime discussed in sect. 1.7.

Having dispensed with the cross-field equation by the fixed-poloidal-field approximation, the flow can be solved on each poloidal field line separately. The solution of this problem is determined by eqs. (1.30), (1.20), (1.13) above. On each of the field lines, η, $\varpi_{\rm A}$ and E are constants, still to be found from the solution. It turns out (Sakurai, 1985) that the problem is visualized conveniently in a space in which the coordinates are s, the arc length along a poloidal field line, and ρ, the gas density. The Bernoulli equation can then be read as an algebraic equation specifying a relation beteen ρ and s. This relation is the solution of the problem. To see this, note that for each field line, $B_{\rm p}$ is a known function of s, and

ϖ is a known function of s through the known shape of the poloidal field lines. Hence with (1.13) the first term in (1.30) is of the form $v_{\rm p}^2/2 = f_1(s,\rho;\eta)$. In this notation, the semicolon separates the the coordinates s,ρ from the parameters $\eta, E, \varpi_{\rm A}$. With the rotation rate Ω of each field line specified, eqs. (1.20),(1.21) show that the second term is of the form $v_\phi'^2/2 = f_2(s,\rho;\varpi_{\rm A})$. The gravitational and centrifugal terms are functions of s only, and the thermal term is of the form $f_3(\rho;K)$ in the polytropic case, or $f_3(\rho;c_{\rm s})$ in the isothermal case. The conditions at the surface of the disk have to be known to solve the problem, so we may assume that the values ρ_0, p_0 of the pressure and density at some point near the base ($s=0$) of the flow are known. One of these 2 values then determines K or $c_{\rm s}$ directly while the other, ρ_0 say, fixes (through the solution of the problem) a relation between the unknown constants $(\eta, \varpi_{\rm A}, E)$. Thus, for a solution of the problem, two more conditions are needed to specify all three constants. These are two critical point conditions, which appear as follows.

1.5.1 Critical points

Writing the Bernoulli equation in the form

$$H(s,\rho;\eta,\varpi_{\rm A}) = E, \tag{1.36}$$

the solution curve $\rho(s)$ can be regarded as a contour line of the Bernoulli function H in the s,ρ plane. The astrophysically relevant solutions start at a very high density near the disk surface, and decrease to vanishing density at infinity. We are therefore interested in unbroken contours of H which cover the entire ρ coordinate. H has 'mountain ranges' however, and brief inspection will show that these mountain ranges can be crossed by a level countour only through mountain passes. These mountain passes are critical points of the saddle type. As we shall see, there are two of these points, and the solution has to cross both. The elevation of H at one of the points determines the value of E. For the solution also to cross the other point, this point must have the same elevation. This will in general be the case only for certain combinations of the parameters $\eta, \varpi_{\rm A}$. Together with the given value of ρ_0, the two critical points thus determine the unknown parameters η, $\varpi_{\rm A}$ and E and the problem is solved.

Notice that there is no need to solve any differential equations, the whole magnetic wind problem is algebraic, for any configuration of the poloidal field (as long as it is prescribed in advance).

It remains to be shown that there are two relevant critical points. At a critical point we have

$$\partial H/\partial s = 0, \quad \partial H/\partial \rho = 0. \tag{1.37}$$

Substituting $v_{\rm p}$ and $v_{{\rm p}\phi}$ from (1.13) and (1.20) one finds that

$$\rho\frac{\partial H}{\partial \rho} = -\frac{v_{\rm p}^4 - v_{\rm p}^2(c_{\rm s}^2 + v_{\rm Ap}^2 + V_{{\rm A}\phi}^2) + c_{\rm s}^2 v_{\rm Ap}^2}{v_{\rm p}^2 - v_{\rm Ap}^2}, \tag{1.38}$$

where $v_{\rm Ap}$, $v_{{\rm A}\phi}$ are the Alfvén speeds based on the poloidal and toroidal field strengths, respectively:

$$v_{\rm Ap} = \frac{B_{\rm p}^2}{4\pi\rho}, \quad v_{{\rm A}\phi} = \frac{B_\phi^2}{4\pi\rho}. \tag{1.39}$$

To interpret the expression for $\partial H/\partial\rho$, note that the dispersion relation for magnetosonic waves in a homogeneous medium is (e.g. Plumpton and Ferraro, 1966):

$$u^4 - u^2(c_{\rm s}^2 + v_{\rm A}^2) + c_{\rm s}^2 v_{\rm A}^2 \cos^2\theta = 0, \tag{1.40}$$

where

$$u = \omega/k \tag{1.41}$$

is the wave speed[3], and θ the angle between the magnetic field vector and the direction of the wave vector $\mathbf{k}$. Thus, $\partial H/\partial\rho = 0$ when the poloidal velocity equals the speed of a magnetosonic wave propagating parallel to the poloidal flow (so that $\cos\theta = B_{\rm p}/B$). Thus (1.38) can be written as:

$$\rho\frac{\partial H}{\partial\rho} = -\frac{(v_{\rm p}^2 - v_{\rm sp}^2)(v_{\rm p}^2 - v_{\rm fp}^2)}{v_{\rm p}^2 - v_{\rm Ap}^2}, \tag{1.42}$$

Where $v_{\rm sp}$ and $v_{\rm fp}$ are the solutions of (1.40) for $\cos\theta = B_{\rm p}/B$. Critical points therefore occur when the flow just balances the speed of a magnetosonic wave propagating opposite to the flow. They are called the slow mode critical point and fast mode critical point, or slow and fast point, for short. In addition to these critical points, there is a singular point of a different kind at $|v_{\rm p}| = v_{\rm Ap}$. Note that only the slow and fast mode critical points yield constraining relations for the solution, the Alfvén point does not yield an additional constraint. Through its appearance in the denominator in (1.42), the Alfvén point is a node rather than a saddle point; all solutions which pass through the slow and fast points also pass through the Alfvén point. This is because a critical point condition has already been applied at the Alfvén point in deriving (1.21). The Alfvén point, however, plays a new role as a critical point when the cross-field balance is considered (sect. 1.6).

The practical problem of determining the location of the critical points and computing the full solution depends a bit on the character of the poloidal field specified. A simple case is the Weber and Davis (1967) model. This is discussed further in sect. 1.7 below.

1.5.2 Multiple critical points

Since the position of the critical points depends on the geometry of the poloidal field configuration, one may wonder if there could not be more than just 2 critical points. H could have an additional mountain range such that there are two slow points and a fast point, for example. Since each critical point adds a condition that has to be satisfied by the flow, and the problem is just closed with two

[3] magnetosonic waves, though anisotropic, are nondispersive.

critical point conditions, one might think such multiplicity is excluded. The flow, however, has a way of generating additional degrees of freedom. Except in carefully construed cases, a supersonic flow develops a shock at a location where it is forced to decelerate. Thus, if the shape of the poloidal field is sufficiently complex that it forces the flow to decelerate somewhere, a shock is formed near that location. This can happen if the flow diverges sufficiently rapidly due to a decrease in poloidal field strength, or if the path of the field line is such that it takes the flow up and down theeffective potential (gravitational plus centrifugal) more than once. The Hugoniot conditions will fix the properties of this shock, but the position of the shock is determined only if one more condition is imposed. The flow can pass through several critical points in such a way that each additional critical point is associated with a shock. After each shock, the flow is reaccelerated and passes though a new critical point. The regularity condition at the additional critical point determines the position of the shock. There are two kinds of shocks in magnetohydrodynamics, named slow and fast shocks (e.g. Jeffrey and Taniuti, 1964), so that the formation of shocks can in principle take place in association with additional slow critical points, as well as with additional fast points. An example of an additional slow point in a realistic disk field geometry is given in Cao and Spruit (1994). Cases with multiple fast points are discussed in Heyvaerts and Norman (1989).

1.5.3 Launching of the wind: the sonic point

If the flow is to be strongly accelerated, the Alfvén point must be at a large distance, and this requires the field to be strong enough to enforce corotation out to that large distance. In this case, it is a good approximation to assume that the Alfvén speed is large compared to the sound speed, at the base of the acceleration region. The slow mode speed, measured at the slow mode critical point, is then close to the sound speed, and the slow mode has the character of a sound wave guided along the field line. For this reason, the slow point is also called the sonic point. Without loss of physical generality, I equate the slow mode speed to the sound speed for the rest of this section.

The importance of the sonic point for the wind problem is that it regulates the *mass flux* on the field line; it governs how much mass is 'launched' into the accelerating region. At the sonic point, $v_{\rm p} = c_{\rm s}$, and the mass flux (per unit area) is

$$\dot{m} = (\rho c_{\rm s})_{\rm c}, \tag{1.43}$$

where the index $_{\rm c}$ means evaluation at the sonic point. The sound speed can be assumed to be known, either explicitly if an isothermal model is used, in general by the energy balance model used. The mass flux is then known if the density at the sonic point is known. At the sonic point, the pressure balance along the flow is affected by hydrodynamic forces, but in the subsonic region before the sonic point their influence is small. As a fair (order of magnitude) approximation, we can take the pressure distribution to be *hydrostatic* between the foot point (index $_0$) and the sonic point, and supersonic beyond. An estimate of the mass flux is

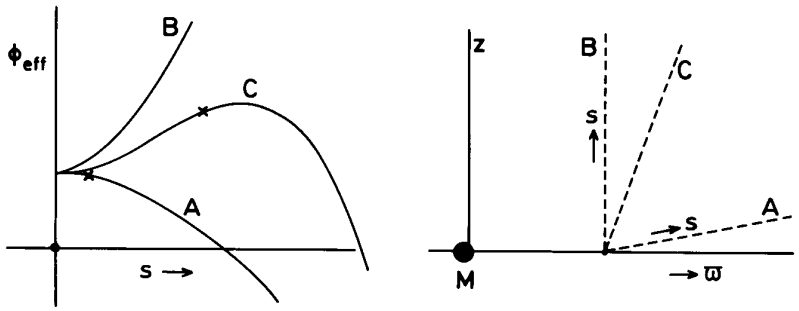

Figure 1.7: Variation of the effective potential with arc length along field lines of different inclinations.

then obtained as

$$\dot{m} \approx \rho_0 c_s \exp[-(\Phi_{ec} - \Phi_{e0})/c_{sc}^2] \tag{1.44}$$

where the temperature has been approximated as constant, and Φ_e is the effective potential including the centrifugal term,

$$\Phi_e(s) = -\frac{GM}{r(s)} - \frac{1}{2}\Omega^2 \varpi^2(s). \tag{1.45}$$

To complete the estimate, we need a value for the potential at the sonic point. Assume that the potential has a maximum, measured along the field line; first increasing due to the gravity of the central object, and then decreasing due to the centrifugal force. Along the increasing part, the density is stratified nearly hydrostatically. Approaching the maximum, the mass starts flowing when the thermal energy in the gas becomes comparable to the distance to the top of the potential barrier. At low temperatures, this happens close to the maximum of the potential. An approximate mass flux is therefore found from (1.44) by taking for Φ_{ec} the maximum of Φ_e. For higher temperatures, the sonic point occurs somewhat before the maximum of the potential. In the absence of rotation the potential is due to gravity alone, and its maximum is at infinity. In this case, the sonic point occurs roughly at the point where the thermal energy is equal to the depth of the gravitational potential. Such a flow is a thermally driven wind, like the Sun's (e.g. Foukal, 1990). At low temperatures, the mass flux is very sensitive to the height of the potential barrier, since it comes in exponentially.

For an understanding of the launching of the wind from a disk, we have to look more closely at the variation of the effective potential near the base of the flow. In fig. 1.7 the variation of the potential is sketched for three paths starting at the same point at the midplane of the disk. If the path is vertical (B), the potential increases monotonically, there is no maximum sufficiently close to the disk surface, and at best a feeble thermally driven wind is possible. At an intermediate inclination (C), there is a maximum near the disk surface, and conditions for launching a wind can be good, depending on the temperature of the gas. Along a path close to the

surface (A), the effective potential *decreases monotonically*. In this case, the wind can start right from the disk surface. The boundary between cases (C) and (A) occurs when the potential curves neither up nor down at the foot point $s = 0$ (see fig. 1.7), i.e. when

$$\partial^2 \Phi_e / \partial s^2|_{s=0} = 0. \tag{1.46}$$

Assuming the foot point to rotate at the Keplerian rate $\Omega = (GM/\varpi_0^3)^{1/2}$, we find

$$\partial^2 \Phi_e / \partial s^2|_{s=0} = \Omega^2 (\sin^2\theta - 3\cos^2\theta), \tag{1.47}$$

where θ is the angle between the field line and the ϖ axis. Thus the boundary occurs at a critical angle (Blandford and Payne, 1982):

$$\theta_c = \mathrm{atan}(\sqrt{3}) = 60^\circ. \tag{1.48}$$

The dependence on field line inclination is summarized in fig. 1.8. On field lines more vertical than 60°, the situation is like in a stellar wind: there is a potential barrier to overcome, and this requires the existence of a hot atmosphere (temperatures comparable to the virial temperature). For inclinations less than 60°, on the other hand, there is no impediment to the flow at all, and one would expect a large mass flux. This is, in fact, somewhat problematic, as discussed further in section 1.7, where the consequences of large mass fluxes are investigated. In between, there is a range in field inclinations (a narrow range if the disk atmosphere is cool compared with the virial temperature), where a reasonable mass flux results, and the magnetic wind theory works best. The detailed solutions of Königl (1989) are of this type. It has been argued (Lubow et al. 1994) that the strong dependence of mass flux on inclination makes the flows in this range unstable. If this is the case, stationary magnetically accelerated flows may not exist, at least not from cool disks. The conditions for stationary flows may be better in AGN. Here, the likely presence of an ion supported torus (with ion temperature near the virial temperature, Rees et al. 1982) near the black hole would allow a magnetically generated flow from a wider range of field line inclinations.

From this discussion, it will be clear that the details of how the wind is launched depend somewhat critically on things which are not presently known in detail, namely the inclination of the field lines near the disk surface and the presence or absence of a hot atmosphere.

1.5.4 Geometry of the magnetic field near the disk

In view of its importance for the wind launching problem, one would like to know what determines the shape of the field lines near the disk surface. Since the field is close to a potential field near the surface, its strength and geometry in this region, including the inclination, is determined uniquely by a boundary condition at the disk surface[4], namely the vertical component of the field strength. There are two

[4] A boundary condition at large distance is also needed. Since the field strength in the disk is likely to be much larger than in the interstellar medium, it is sufficient to take a standard condition of vanishing field strength at infinity.

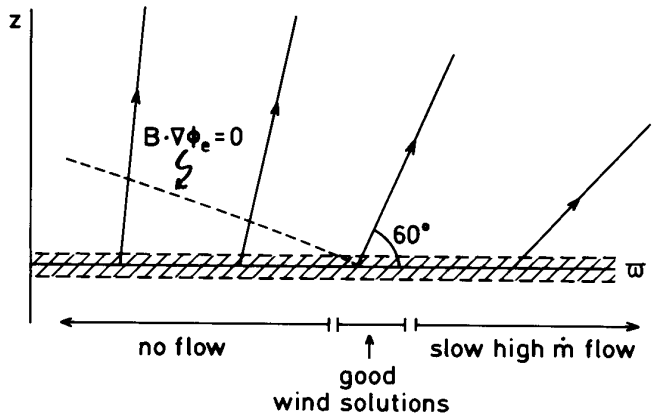

Figure 1.8: Launching conditions of a wind on field lines with varying inclination. The maximum of the effective potential along field lines is shown by a broken line. If the disk is cool, only a narrow range of inclinations around 60° yields 'good' wind solutions. The slow, high $\dot{m}$ flows at low inclination are problematic, see text.

possibilities for the origin of this field. If there is a dynamo process acting in the disk, one may expect field strengths of the order of equipartition with the gas pressure, as numerical simulations show (Hawley et al. 1995, Brandenburg et al. 1995). These simulations also indicate that the field is created with small length scales L, of the order of the disk thickness, in the radial direction, and somewhat longer in the azimuthal direction. The potential field created by such a small scale field decays with distance above the disk like $\exp(-z/L)$. This would not be the ideal field for driving magnetic winds.

Another possibility is that the field is not internally generated, but is due to magnetic flux captured from the environment in during formation of the disk, and advected and compressed by the accretion process. Poloidal flux captured in this way cannot be destroyed by local processes in the disk, it can only escape by diffusing radially outward. The field strength would then be determined by the balance between outward diffusion and inward accretion (van Ballegooijen 1989, Spruit 1994). In the absence of a theory for (turbulent) diffusion in an accretion disk, it is not possible to predict with any reliability what distribution of field strengths will result. Since all energy densities in the disk increase inward however, including that of the accretion flow, it is reasonable to assume that the balance will yield a field with inward increasing strength. The field above the disk will then have a shape like that suggested by fig. 1.8. In Spruit et al. (1995) we have argued that fields of this configuration can be quite strong, with magnetic energy densities exceeding the gas pressure, which would make them ideal for the production of magnetic outflows.

1.5.5 Poynting and kinetic energy fluxes

The wind carries both kinetic and magnetic energy. The asymptotic ratio of these, at large distance, is a measure of how 'magnetic' the wind is. The Poynting flux, in the MHD approximation, is

$$\mathbf{S} = \frac{1}{4\pi}(\mathbf{v}\times\mathbf{B})\times\mathbf{B}. \tag{1.49}$$

The relevant component of $\mathbf{S}$ is that parallel to the poloidal flow. With (1.14) and (1.15), this can be written as

$$S = \frac{1}{4\pi}\Omega(\boldsymbol{\varpi}\times\mathbf{B})\times\mathbf{B}\cdot n, \tag{1.50}$$

where $\mathbf{n}$ is a unit vector along $\mathbf{v}_{\rm p}$. Working out the cross products:

$$S = \Omega\varpi\frac{B_{\rm p}B_\phi}{4\pi}. \tag{1.51}$$

Thus, the Poynting flux can be read as the work done by the rotation against the magnetic torque. At large distance, the azimuthal velocity (in the inertial frame) is small compared with $\Omega\varpi$, so that by (1.15) $B_p \approx B_\phi v_p/\Omega\varpi$, and $B_\phi \gg B_{\rm p}$. Thus

$$q \equiv \frac{S}{K}|_\infty = \frac{B_\phi^2}{2\pi\rho v_p^2}|_\infty = 2\frac{v_{\rm A}^2}{v_{\rm p}^2}|_\infty, \tag{1.52}$$

where K is the kinetic energy flux $\frac{1}{2}\rho v^2$. Many flows (an example is the cold Weber Davis model, sect. 1.7) have their fast mode critical point at infinity so that $(v_{\rm A}/v_{\rm p})_\infty = 1$, and $q = 2$. The magnetic and kinetic energy fluxes are then comparable at infinity. Near the disk, the Poynting flux dominates. Part of the Poynting flux is converted into a kinetic energy flux during the acceleration process.

Relation (1.52) is valid only if the field survives in a highly wound-up form asymptotically. In section 1.9 I will argue that nonaxisymmetric instabilities are likely to destroy at least part of the toroidal field. In reality, the magnetic contribution to the energy flux may therefore be rather unimportant, and $q \ll 1$ rather than of order unity. If this is the case, we have the aesthetically pleasing result that the magnetic acceleration process, after all its internal workings, produces a basically ballistic wind, which is only moderately magnetic.

1.5.5.1 electron-positron flows

There is some observational evidence for outflows containing electron-positron pairs ($e^\pm$) from relativistic objects. In the galactic center source 1E1740.7-2942 a positron annihilation feature has been observed (Churazov et al. 1991, Churazov et al. 1994), and a transient feature has been seen in X-ray Nova Muscae (Gil'fanov et al. 1991). Thus there appear to be pair producing as well as jet producing black hole candidates (though no case is known yet which combines both), and it

is natural to speculate that magnetic jets may exist that consist predominantly of a pair plasma. The Blandford-Znajek mechanism is thought to produce such flows (Blandford 1993 and references therein). Such a flow is technically not different from the jets considered above, since the same MHD equations apply. The main difference is that pairs may annihilate, thus removing mass and inertia from the flow. This would tend to increase the relative importance of the Poynting flux in the flow. At the same time, however, the Alfvén speed would increase due to the decreasing mass density, and speed up the instability of the toroidal field. As the mass disappears, the magnetic field would therefore also disappear. In the non-relativistic case, the flow would then decay completely into photons. If the flow is relativistic, it is possible that part of the energy of the decaying field is converted into a flux of low-frequency electromagnetic waves. For recent speculations on this topic, see Levinson and Blandford (1995). A magnetically driven pair plasma flow from a pulsar has been invoked by Arons and collaborators (Gallant and Arons 1994) for the Crab nebula.

1.6 Cross-field balance

The collimation of the flow is determined by the force balance in meridional planes, in the direction perpendicular to the field. The stationary, axisymmetric equation of motion that governs this balance is called the Grad-Shafranov or Grad-Schlüter-Shafranov equation. For our case of a magnetized flow it has a somewhat complicated form. Some important aspects are discussed below, but for details I refer to Heinemann and Olbert (1978) and Sakurai (1985). To begin with, note that the solutions obtained in the above for a fixed poloidal field are still valid for the full problem, provided we read them as relations expressing the solution in terms of the (yet to be determined) poloidal field.

The solutions of the azimuthal and longitudinal equations of motion are (1.20) [with (1.21)] and (1.30). Inserting these into the original equation of motion (1.4), we get the required expression for the remaining, perpendicular, component. The result is (Heinemann and Olbert 1978, Okamoto 1975, 1992):

$$\begin{aligned} 0 \;=\; & \nabla\psi \left\{ \mathrm{div}\left[\left(\frac{\eta^2}{\rho}-\frac{1}{4\pi}\right)\frac{\nabla\psi}{\varpi^2}\right] - \rho\left(E' - \frac{1}{\gamma-1}\frac{p}{\rho}\frac{K'}{K} + \varpi^2\Omega\Omega'\right)\right. \\ & \left. -\frac{B^2}{\rho}\eta\eta' - \varpi B_\phi\left[(\eta\Omega)' - \frac{1}{\varpi^2}(\eta\Omega\varpi_{\mathrm{A}}^2)'\right]\right\}, \end{aligned} \tag{1.53}$$

where a prime $'$ denotes $\mathrm{d}/\mathrm{d}\psi$. It follows that the expression in braces must vanish. This equation is to be read as a two-dimensional partial differential equation for the stream function $\psi(\varpi, z)$ of the poloidal field. Note that it is a somewhat implicit kind of equation, since it involves the quantities $E(\psi), K(\psi), \varpi_{\mathrm{A}}(\psi)$ which are known in terms of ψ only as solutions of eqs. (1.20) and (1.30). Hidden in (1.53) is the fact that it is singular at the Alfvén point. By working out the coefficient of the highest (second) derivatives, one finds that it vanishes at the Alfvén point, so a regularity condition must be applied there. An additional complication in solving the equation is that it is of mixed type, namely elliptic in some parts of

the (ϖ, z) space and hyperbolic in others. Where the boundaries are is found out by computing the characteristics of eq. 1.53. This is conveniently done by inserting a short wave approximation:

$$\nabla\psi = \mathbf{k}\psi, \tag{1.54}$$

and keeping only the highest (quadratic) terms in $\mathbf{k}$. If $k_\parallel$ and $k_\perp$ are the components of $\mathbf{k}$ parallel and perpendicular to $\mathbf{B}_\mathrm{p}$, this highest order treatment of the equation turns out to yield

$$\frac{k_\parallel^2}{k_\perp^2} = \frac{(v_\mathrm{p}^2 - v_\mathrm{cp}^2)(c_\mathrm{s}^2 + v_\mathrm{A}^2)}{(v_p^2 - v_\mathrm{sp}^2)(v_p^2 - v_\mathrm{fp}^2)}, \tag{1.55}$$

where a new critical velocity v_cp has appeared:

$$v_\mathrm{cp}^2 = \frac{c_\mathrm{s}^2 v_\mathrm{Ap}^2}{c_\mathrm{s}^2 + v_\mathrm{A}^2} = \frac{v_\mathrm{sp}^2 v_\mathrm{fp}^2}{v_\mathrm{sp}^2 + v_\mathrm{fp}^2}. \tag{1.56}$$

As the flow accelerates it first meets an elliptic region ($k_\parallel^2/k_\perp^2 < 0$) for $v_\mathrm{p} < v_\mathrm{cp}$, then a hyperbolic region for $v_\mathrm{cp} < v_\mathrm{p} < v_\mathrm{sp}$, another elliptic region $v_\mathrm{sp} < v_\mathrm{p} < v_\mathrm{fp}$, and finally another hyperbolic region for $v_\mathrm{p} > v_\mathrm{fp}$. The significance of the critical velocity v_cp is seen by noting that it is the speed of the *cusp* of an axisymmetric slow mode wave (Heinemann and Olbert 1978). The surface on which $v_\mathrm{p} = v_\mathrm{cp}$ is called the cusp surface. The cusp speed does not appear in the case of a prescribed poloidal field, since the wave mode involved bends the poloidal field lines.

The characteristics of eq. 1.53 should not be confused with the characteristics of a time dependent MHD problem. Though various wave speeds appear, one is dealing with a time-independent flow. The ellipticity or hyperbolicity of the problem refers to characteristics in the (ϖ, z) space, not in an $(\mathbf{r}, t)$ space. Physically, however, there is a clear relation of the boundaries between elliptic and hyperbolic regions in the stationary problem on the one hand, and wave speeds in a time dependent problem on the other. This comes about because a wave in a frame comoving with the fluid appears as a stationary flow in the rest frame if the flow speed just cancels the propagation of the wave. This happens at the critical points.

The presence of 4 different regions poses practical problems when constructing numerical solutions. The singular point at $v_\mathrm{p} = v_\mathrm{Ap}$ has to be dealt with, as well as the boundaries between elliptic and hyperbolic regions, since different discretization schemes have to be used in each for numerical stability. The lower boundary condition at the disk surface, together with the regularity condition at the Alfvén surface act as the boundary conditions for the elliptic regions (even though the boundaries of these regions do not coincide with these surfaces!). The solutions in the inner and outer hyperbolic regions are determined with values at the cusp and fast surfaces as initial data, respectively. If $B_\phi \ll B_\mathrm{p}$ near the sonic point, the first hyperbolic region is quite narrow, and does not play an important role. One can then regard the entire region inside fast magnetosonic surface as elliptic, also in practical solution algorithms. This is the case when the field is strong enough that 'interesting' degrees of acceleration take place. For discussions on numerical procedures, see Sakurai (1985, 1987) and Camenzind (1987).

1.7 The character of the wind at high and low $\dot{m}_{\rm w}$

A simple model which demonstrates important parts of the physics is that of Weber and Davis (1967). I review it here in particular to discuss the dependence of the wind problem on the mass flux. This also relates to the question what happens to the flow when the inclination of the field line to the disk surface is less than 60° (cf. sect. 1.5.3).

The model takes the poloidal field to be purely radial (in spherical coordinates), and looks only at the equatorial plane (with respect to the rotation axis)[5]. Though the model was invented for stellar winds, it can also be applied to the case of disk winds on low inclination field lines, nearly parallel to the disk surface. To further simplify the problem, I ignore the thermal pressure ('cold' limit), so that all acceleration is magnetic.

Because he poloidal field is radial, its strength is given by

$$B_{\rm p} = B_0(\varpi_0/\varpi)^2, \tag{1.57}$$

where ϖ_0 is the foot point of the field line on the disk, which we assume to rotate at the Keplerian rate $\Omega = (GM/\varpi^3)^{1/2}$. For the analysis it is practical to normalize ϖ and ρ to their values at the Alfvén point, by introducing the variables

$$x = \varpi/\varpi_{\rm A}; \qquad y = \rho/\rho_{\rm A}, \tag{1.58}$$

and a normalized Bernoulli function

$$\tilde{H} = H\frac{\varpi_{\rm A}}{GM}. \tag{1.59}$$

Substituting (1.20) into (1.30), the Bernoulli equation then takes the form

$$\tilde{H}(x,y) = \frac{\beta}{2x^4y^2} + \frac{\omega}{2}\frac{(x-1/x)^2}{(y-1)^2} - \frac{1}{x} - \frac{\omega}{2}x^2 = E, \tag{1.60}$$

where

$$\beta = \frac{B_0^2\varpi_0^4}{4\pi GM\rho_{\rm A}\varpi_{\rm A}^3} = \left[v_{\rm Ap}^2/\frac{GM}{\varpi}\right]_{\rm A}, \qquad \omega = \frac{\Omega^2\varpi_{\rm A}^3}{GM} = \left[\Omega^2\varpi^2/\frac{GM}{\varpi}\right]_{\rm A}. \tag{1.61}$$

Since the sound speed vanishes, $v_{\rm p} = 0$ at the sonic point, and the gas density diverges there. With (1.20) the azimuthal velocity v'_ϕ then vanishes also. Near the sonic point, the first two terms in (1.60) describing the kinetic energy therefore vanish, and the only terms left are the gravitational and centrifugal ones. The condition $\partial_x H = 0$ then yields $\omega = x_s^{-3}$, in dimensional terms $GM = \Omega^2\varpi^3$. Thus, the sonic point x_s is at the foot point $x_0 = \varpi_0/\varpi_{\rm A}$ of the field line, and

$$x_0 = \omega^{-1/3}. \tag{1.62}$$

[5] A purely radial field smacks of monopoles. To remedy this, the field below the equator is given the opposite sign of the field above. The resulting configuration, with a current sheet at the equator, is physically realizable. For the dynamics of the wind, the sign of the magnetic field is unimportant. This is called the 'split monopole' configuration.

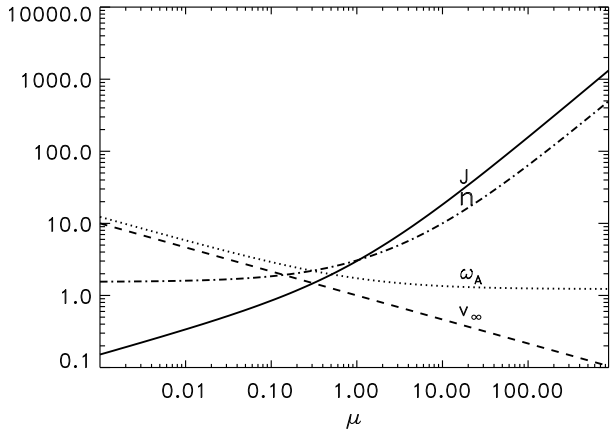

Figure 1.9: The cold Weber-Davis model, showing Alfvén radius $\omega_{\rm A} = \varpi_{\rm A}/\varpi_0$, angular momentum flux $J = \dot{J}/(\eta_*\Omega\varpi_0^2)$, asymptotic flow speed $v_\infty/\Omega\varpi_0$, and field angle $n = (B_\phi/B_{\rm r})_{\rm A}$ as functions of the mass flux.

The value of the Bernoulli function is now also known,

$$E = -\frac{1}{x_0} - \frac{1}{2}\omega x_0^2 = -\frac{3}{2}\omega^{1/3}. \tag{1.63}$$

The relation between β and ω follows from the fast point condition. It turns out that the fast point is at infinity (Goldreich and Julian 1970). We skip this part of the derivation. One finds then that x^2y remains finite at infinity, which corresponds to the fact that the flow speed reaches a finite value at infinity. Using the conditions $\partial_y H = \partial_x H = 0$ for the fast point, and the Bernoulli equation, all expanded for $x \to \infty$, the result is

$$(x^2y)_{\rm f} = \frac{2}{3} - \omega^{-2/3}, \tag{1.64}$$

$$\beta = \omega(\frac{2}{3} - \omega^{-2/3})^3. \tag{1.65}$$

We need to express this result in more physical terms. For a given field strength and rotation rate, the external parameter determining the solution is the density at the base of the flow or, equivalently, the mass flux. Consider the mass flux as the external parameter. It is measured by the quantity $\eta = \rho v_{\rm p}/B_{\rm p}$ [cf. (1.13)], the mass flux 'per field line'. This has the dimension of the square root of a density. In fact, evaluating it at the Alfvén point,

$$\eta = \left(\frac{\rho_{\rm A}}{4\pi}\right)^{1/2}. \tag{1.66}$$

The quantity

$$\eta_* \equiv \frac{B_0}{4\pi\Omega\varpi_0} \tag{1.67}$$

has the same dimension. It turns out to be the natural unit of mass flux in the model. It increases with the field strength, reflecting the fact that a stronger field is able to accelerate a larger mass flux to the same speed. Defining a dimensionless mass flux μ:

$$\mu = \eta/\eta_*, \tag{1.68}$$

we want to express the results as functions of this dimensionless flux. From the definition of β, and using (1.62), we find that

$$\beta = (\mu^2\omega)^{-1}. \tag{1.69}$$

Hence with (1.65):

$$\omega = [\frac{3}{2}(1+\mu^{-2/3})]^{3/2}. \tag{1.70}$$

The location of the Alfvén point is then

$$\varpi_{\rm A}/\varpi_0 = \omega^{1/3} = [\frac{3}{2}(1+\mu^{-2/3})]^{1/2}. \tag{1.71}$$

When the mass flux is small, $\mu \ll 1$, the Alfvén radius is far from the origin of the flow. For large mass fluxes, $\mu \gg 1$, $\varpi_{\rm A}$ does not get arbitrarily close to ϖ_0, but reaches the minimum value

$$\varpi_{\rm A} = \varpi_0(3/2)^{1/2} \quad (\mu \to \infty). \tag{1.72}$$

Further quantities of interest are, for example, the angular momentum flux per field line:

$$\dot{J} = \eta\Omega\varpi_{\rm A}^2 = \eta_*\Omega\varpi_0^2\,\mu\frac{3}{2}(1+\mu^{-2/3}). \tag{1.73}$$

This gives the angular momentum flux in terms of the mass flux and the conditions at the base of the flow. The terminal speed of the flow follows from (1.13) and (1.64):

$$\frac{v_\infty}{\Omega\varpi_0} = (\beta\omega)^{1/6} = \mu^{-1/3}. \tag{1.74}$$

This demonstrates one of the most important properties of the magnetic acceleration model: it can produce wind speeds that exceed the escape speed $\Omega\varpi_0$ from the rotating object. In principle, it can accelerate a sufficiently small mass flux to arbitrarily large speeds, though in practice this ability is limited by the rather weak 1/3 power in (1.74).

For $\mu = 1$, the final speed is just equal to the rotation velocity at the base of the wind, and for large mass flux, the final speed becomes *arbitrarily small*. What kind of flows are these massive but sluggish winds? A good way to see this is by evaluating the pitch angle of the field at the Alfvén point. The model gives for this

$$\left(\frac{B_\phi}{B_{\rm p}}\right)_{\rm A} = (2-3\omega^{1/3}-\beta+\omega)^{1/2}\beta^{-1/2}. \tag{1.75}$$

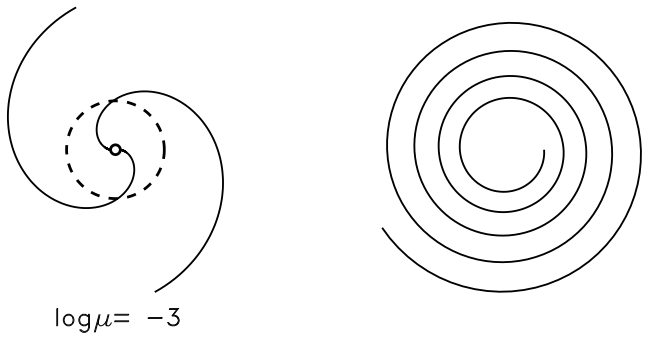

Figure 1.10: Shape of the field lines in a cold Weber-Davis model for low (left) and high (right) mass loss cases. Dashed line: Alfvén radius.

The limiting forms are

$$\left(\frac{B_\phi}{B_{\rm p}}\right)_{\rm A} \approx (19/8)^{1/2} \quad (\mu \ll 1) \qquad (1.76)$$
$$\approx 1.14\mu \quad (\mu \gg 1).$$

For small mass loss, the pitch angle of the field at the Alfvén radius reaches a constant value which happens to be very nearly one radian. For large μ however, the azimuthal field dominates over the poloidal field. This is illustrated in fig. 1.10, showing the shape of the field lines for a large and a small value of μ. The case $\mu \ll 1$ can be properly called a centrifugally accelerated flow. Up to the Alfvén radius, the field lines are not strongly bent, the flow corotates approximately, and the poloidal flow speed can be found to good accuracy from the effective potential. Beyond the Alfvén radius corotation fails, so that the effective potential is not a good estimator for the flow speed any more. For high mass loss, the situation is very different. Corotation now fails right from the start, so that a strongly wound up ($B_\phi \gg B_p$) field develops long before the Alfvén radius is reached. The flow is slowly 'pushed' outward by the pressure of the toroidal field, with final speeds much less than Ωr_0. Rather than being 'flung out', the flow is more a sequence of magnetostatic equilibria, since the flow time scale $\varpi/v_{\rm p}$ is much longer than the dynamical time scales $(GM/\varpi^3)^{-1/2}$ and $\varpi/v_{\rm A}$. At the Alfvén point ($v_{\rm p} = v_{\rm Ap}$), for example, the ratio of the flow and Alfvén time scales is $v_{\rm A}/v_{\rm p} = B_\phi/B_{\rm p} \sim \mu$. This disparity of time scales brings in the question of stability. If it is unstable, the highly wound-up field will change on the short Alfvén time scale, interfering with its pushing activity. For the low-μ centrifugal case, the field is not strongly twisted, and stability is not an issue, until the flow reaches the Alfvén radius. By then, most of the acceleration has already taken place. I return to the question of stability in sect. 1.9.

1.7.1 Relativistic flows

The relativistic case is somewhat outside the scope of this text. I will discuss a few basic properties of the special-relativistic case, and refer to Michel (1973), Goldreich and Julian (1970) and Li, Chiueh and Begelman (1992) for details, and Bekenstein and Oron (1978), Okamoto (1978,1992) and Camenzind (1987) for the general relativistic treatment. Also left out is the Blandford-Znajek model for magnetic flows driven by the rotation of a black hole. See Blandford (1993) and references therein.

In the nonrelativistic case, the only parameter determining the behavior of the flow was the dimensionless mass loss rate μ; the dependence on the other physical parameters could be found by simple scalings. In the special relativistic case, an additional parameter $w = \Omega\varpi_0/c$ appears because the speed of light now fixes a velocity scale. Neglecting the gas pressure, a Bernoulli equation can again be derived as in sect. 1.4 (the derivation, in the this case, is most easily done in the inertial frame). It can, as before, be written in the form $H(\varpi, \rho) = E$, but analysing it is a bit more complicated. In the extreme-relativistic limit, in which the asymptotic Lorentz factor is large, the equivalent of relation (1.74) becomes

$$\gamma_\infty = \frac{\Omega\varpi_0}{c}\mu^{-1/3}, \tag{1.77}$$

(Michel, 1969), where μ is given by (1.68). As the mass flux is decreased, and γ_∞ increases, the Alfvén radius asymptotically approaches the light cylinder radius c/Ω. The high inertia of the flow at large Lorentz factor ensures that ϖ_A always stays smaller than c/Ω.

Eq. (1.77) shows that the flow can in principle become relativistic even when it is launched from a non-relativistic ($\Omega\varpi_0/c \ll 1$) object, if the mass flux is low enough. In practice, however, the weak dependence on μ means that Lorentz factors larger than a few can be produced only by relativistic objects.

The cross field balance plays a more important role in the acceleration region than in the non-relativistic case. Whereas in the non-relativistic case the assumption of a fixed prescribed poloidal field is still fair near the Alfvén surface, this is not the case for relativistic flows. In the extreme relativistic limit, the inertial forces in the flow are so high near the Alfvén surface that they bend the poloidal field lines into a nearly horizontal shape at ϖ_A (Camenzind 1987).

1.8 Collimation by 'hoop stress'

The curvature force exerted by the toroidal field compresses the field configuration towards the axis. This effect becomes important only when the toroidal field is comparable to or larger than the poloidal field, otherwise the configuration is determined by the internal equilibrium of the poloidal field. For low mass loss flows (cf sect. 1.7), collimation by the hoop stress in the toroidal field therefore starts roughly at the Alfvén radius. The effect was first observed in calculations of the solar wind by Suess and Nerney (1975).

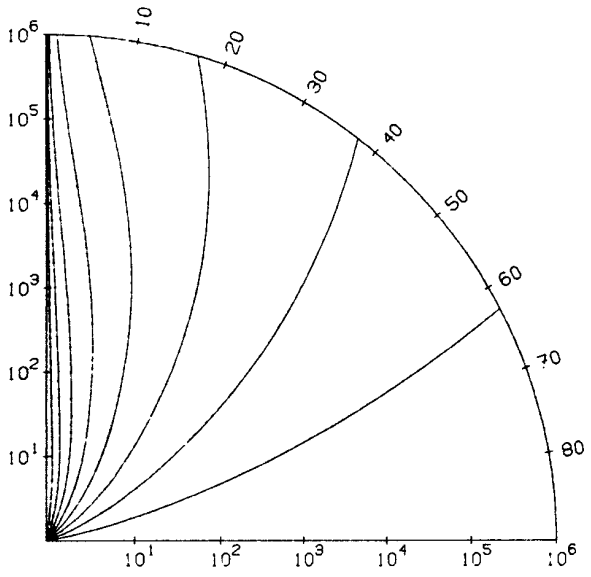

Figure 1.11: Collimation of field lines in an initially spherical stellar wind. Radius scale is logarithmic, in units of the Alfvén radius. All field lines asymptotically become parallel to the axis. The logarithmic distance scale distorts the field lines: on a linear scale the distance of each field line from the axis increases monotonically. From Sakurai (1985).

Note that collimation here is meant in 'optical' sense: a flow is collimated if the flow lines are parallel. This says nothing about the *width* of the flow. For astrophysical jets, however, a collimated jet in practice is also narrow. This is because the central engine is very small compared with the scale of observed jets. An AGN jet for example that expands by a factor 1000 from its expected origin near the central black hole is still less than a parsec across.

The asymptotic collimation of an initially radial flow is illustrated in fig. 1.11. In this model (Sakurai, 1985) a flow is launched spherically symmetric on a 'split monopole' field. After passing through the Alfvén point, the field becomes predominantly toroidal, and this causes the flow to become perfectly collimated (all flow lines parallel to the axis) no matter how small the rotation rate of the star. The rate at which this collimation takes place, however, is slow, requiring several orders of magnitude in distance. For ordinary stellar rotation rates, the distance needed for full collimation is unrealistically large: the flow reaches its interstellar termination shock well before being collimated.

In addition to the perfectly collimated flows like Sakurai's, solutions have been found that are asymptotically uncollimated, in spite of the hoop stress. If the field configuration is such that the field lines diverge sufficiently rapidly near the Alfvén surface (faster than a purely radial field), the fast mode point is located at only a few Alfvén radii, and the flow remains uncollimated (Begelman and Li 1994).

Depending on the conditions in the accelerating region, it seems one either gets an asymptotically fully collimated flow (the 'cylindrical' case) or an uncollimated, space-filling flow (a 'conical' flow, see also Sauty and Tsinganos 1994, Nitta 1994, Tomimatsu 1994, Heyvaerts and Norman 1996). In the latter case, the asymptotic ratio q of magnetic to kinetic energy flux is smaller than in the cylindrical case [where $q = 2$, cf. sect. 1.5.5].

The process of collimation by hoop stress is a natural consequence in axisymmetric rotating winds, and can be computed in detail. The completeness and accuracy suggested by such computations, however, is somewhat misleading because they depend very heavily on the assumption of axisymmetry. If regions of predominantly toroidal field are as unstable as toroidal fields elsewhere in the universe and the laboratory, a significant revision of our picture of the collimation of magnetic winds is in order (sect. 1.5.5).

1.9 Kink instability

In the previous section we found that a predominantly toroidal field develops outside the Alfvén surface. In high mass loss flows, it develops also inside the Alfvén radius. Consider first the case of a low-μ flow, outside the Alfvén surface. Assume that the flow is well collimated, and move into a frame comoving with the flow. In this frame, we see a toroidal field, slowly decreasing in time by the expansion of the flow. A predominantly toroidal field, however, is violently unstable to kink instabilities: such a configuration is equivalent to the linear pinch (e.g. Roberts 1967, Parker 1979, Bateman 1980). The mechanism of the instability is illustrated in fig. 1.12. An initially axial, untwisted, magnetic field is wound up and becomes unstable when the azimuthal becomes larger than the axial field strength. This is akin to the instability of a twisted rubber band (fig. 1.12a). Instability sets in when the axial tension vanishes. Denoting by B_z and B_ϕ the axial and azimuthal components of the field, the axial component of the stress is $(-B_z^2 + B_\phi^2)/8\pi$. The first term is the net magnetic tension due to the axial field, and is stabilizing; it likes to keep field lines straight. The second term, equal to the magnetic pressure exerted by the azimuthal component, is positive, expansive. When the pressure becomes larger than the tension, some of the energy put in by the twisting is released by a kink. Each kink reduces the number of windings by one, at the expense of increasing the energy in the axial field by lengthening axial field lines somewhat[6].

The kink instability is a transition to a nearby equilibrium of lower energy, i.e. the instability saturates at a finite amplitude. This is because the amount of azimuthal field energy that can be released is finite, while the energy expended lengthening the the axial field increases indefinitely with the amplitude of the

[6] The condition $B_\phi > B_z$ can underestimate the degree of instability. A cylindrical field configuration typically becomes unstable already when it is twisted by more than one full turn, independent of the distance between the surfaces at which the twist is applied (Kruskal-Shafranov condition). In our case, this is not relevant, however, because B_ϕ/B_p increases with distance in such a way that the number of turns in the field is always less than one at the point where B_ϕ first exceeds B_p.

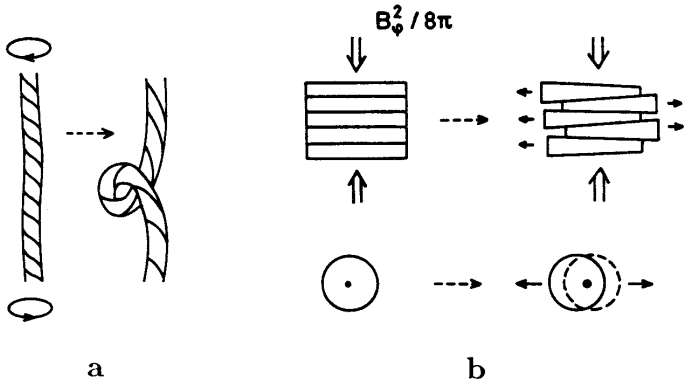

Figure 1.12: Sketch of the kink instability mechanism. a: in analogy with an overtwisted rubber band. b: when the azimuthal field dominates, the instability is like that of a stack of deformable disks under compression.

perturbation. In a predominantly azimuthal field, the instability can also be visualized as shown in fig. 1.12b. A stack of deformable disks (think of the disks in your spinal column, for example) is compressed (by the pressure of the azimuthal field). By slipping sideways and deforming somewhat, the disks can release some of the pressure, at the expense of the integrity of the stack. In stellar interiors, such configurations are also known to be highly unstable in spite of the presence of a stabilizing thermal buoyancy force (Tayler 1980, Pitts and Tayler 1985).

In these descriptions of the instability, the field is treated as if embedded in a neutral medium, and the instability is a so-called 'external' kink. In practice, the flow could be surrounded by, or itself surround, a less twisted field configuration. This has a stabilizing effect. Conditions for instability in this case (the 'internal' kink) are somewhat more complicated. For more on the subject see, e.g. Bateman (1980, Ch. 6)[7].

Kink instability develops on a time scale $\varpi/v_{\mathrm{A}\phi}$, the Alfvén travel time across the flow, based on the azimuthal field strength. The moment that instability takes place, the azimuthal field providing the collimating hoop stress is reduced (see also Eichler, 1993). The energy involved goes into a less ordered field component which, if anything, adds *outward* magnetic pressure instead of an organized force towards the axis. Thus, the collimating effect of B_ϕ decays at the same rate as the instability takes place. The reduction of the collimating hoop stress has the strongest effect in the most collimated flows; this is seen as follows. If the collimation angle is θ, the radial expansion speed of the jet is $v_\varpi = \theta v_{\mathrm{p}} \approx \theta v_{\mathrm{A}}$, which is small compared with the Alfvén speed. Hence the instability has ample

[7] In Bateman, and in the controlled fusion literature, the use of the words 'poloidal' and 'toroidal' in case of cylindrical fields is opposite to our usage; this has to do with the torus geometry assumed there.

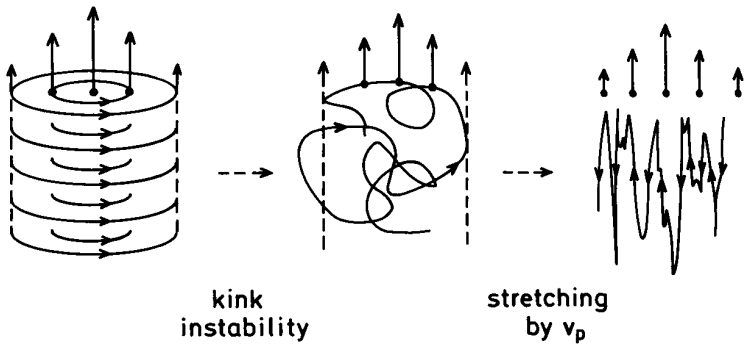

Figure 1.13: Production of a longitudinal field by kink instability. The longitudinal flow is taken to depend on distance from the jet axis. Initially parallel to magnetic surfaces, instability forces the flow to cross the displaced field lines. The differential flow speed stretches the displaced azimuthal field lines along the axis.

time to act as the jet moves outward. The effect of the instability would be less dramatic close to the Alfvén radius. Choudhuri and Königl (1986) have proposed that kink instability near the Alfvén radius may be responsible for some of the alignment anomalies seen in jets at the VLBI scale.

It takes longer than the instability time scale to dissipate the disorganized field component it produces (this is related to the known slow dissipation of magnetic helicity, and is seen also in numerical simulations, e.g. Galsgaard 1995). This dissipation, however, eventually leads to a reduction of the field strength compared with the standard axisymmetric jet. A second consequence of kink instability is therefore that the ratio of magnetic to kinetic energy flux in the jet becomes less than unity (see sect. 1.5.5). Since the Alfvén speed is lower, the fast mode critical point is closer to the source, perhaps at only a few Alfvén radii. Most of the observed jet would then be outside the fast mode point, and kinetic energy dominated. In short: the jet behaves like a ballistic flow, like a water jet from a fire hose. This would simplify the magnetic jet picture considerably: though the acceleration process is intensely magnetic, it would eventually produce a ballistically moving jet in which magnetic stresses are a secondary factor as far as the dynamics is concerned.

Some observational evidence for the action of kink instabilities may be the fact that the magnetic field tends to be parallel to jet axis, at least in the faster (type II) jets (Bridle and Perley, 1984). If the flow speed along the jet is not exactly uniform over its cross section, the irregularities in the field produced by the instability will be stretched along the jet axis, see fig. 1.13. The strength of this longitudinal field will be comparable to the kinetic energy of *differential* velocity across the jet. This field will have many small scale reversals of direction, explaining why the total poloidal magnetic flux inferred from observations (which are not sensitive to the direction of the field lines) is much larger than can be easily accomodated in

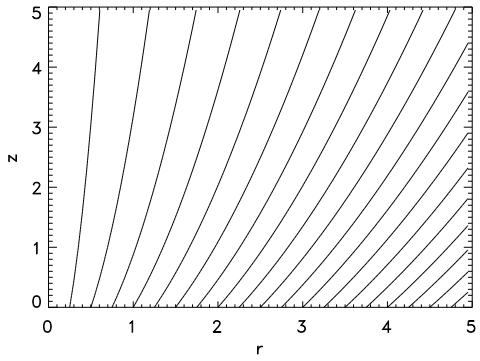

Figure 1.14: Field lines of a potential field produced by a magnetic field strength varying as $(r^2+1)^{-1/2}$ on the disk surface. The collimating shape of the field lines is due to the magnetic flux in the outer parts of the disk.

the accelerating region. These observational indications can equally be explained by stretching of the field by interaction with an external medium, but irregularities produced internally by kinking have the advantage that they will also work in the absence of any interaction with the surroundings.

1.10 Poloidal collimation

In addition to 'toroidal' collimation by hoop stresses, a poloidal magnetic field surrounding the jet can also be a collimator. This is likely to be a powerful effect (Blandford 1993, Spruit 1994) if the disk is 'Large' (where by 'Large' I mean extending over a significant number of decades in radius). As an example to demonstrate this, assume that the vertical field strength at the surface of the disk is of the form

$$B_z \sim (r^2/r_i^2+1)^{-\nu/2}, \tag{1.78}$$

where r_i is the inner edge of the disk and we take ν to be between 0 and 2. Then the field strength is largest in the inner parts of the disk, but the magnetic flux $\int rB_z \mathrm{d}r$ is dominated by the outer regions of the disk. This is a reasonable situation to expect for the field in a disk. A radially selfsimilar disk, for example (Blandford and Payne 1982), has $\nu = 5/4$. In the inner accelerating region of the flow such a field is close to the potential field given by the distribution of flux on the disk surface. It turns out that for a distribution like (1.78), the field lines have a nice, naturally collimating, shape. An example is shown in fig. 1.14 (Spruit 1994), which shows the field lines for the case $\nu = 1$. In this case, the field lines are parabolas, hence their collimation becomes *perfect* at large distance. Of course, the field stops to have this shape near the Alfvén surface and beyond, and at distances where the finite size of the disk becomes noticeable. We can derive a maximum degree of collimation from these ideas, as follows (Spruit, Foglizzo and Stehle 1996). The best collimation is obtained when the Alfvén surface is at a

distance of the order of the disk size, but not further. At larger distances than this, the field more resembles that of a dipole, and does not have any collimating properties. For a field of the form (1.78) one finds (for the case $\nu = 1$) that the angle of the field lines with the axis, at the Alfvén surface, is

$$\theta_{\rm min} \approx (r_{\rm i}/r_{\rm d})^{1/2}, \tag{1.79}$$

where $r_{\rm i}$ and $r_{\rm d}$ are the inner and outer radii of the disk. If we assume that no further collimation takes place beyond the Alfvén surface, for example because of the kink instabilities discussed above, this angle is also the minimum opening angle of the jet. If the Alfvén distance is significantly smaller or larger than $r_{\rm d}$, the collimation is worse.

We can compare these minimum angles of collimation with conditions expected for various kinds of disk. This is shown in table 1.2. This shows that poloidal collimation is capable of explaining opening angles of less than a degree in most systems, with the notable exception of Cataclysmic Variables. And, in fact, no CV is known to produce a jet, though there is evidence for outflows from many such objects (section 1.2). I interpret this as a good case for the importance of poloidal collimation. A nice test case in this context is R Aqr. It consists of a white dwarf accreting from a giant companion, demonstrating that it is not the white dwarf nature of the primaries in CV that prevents them from having jets. Because of its very long orbital period, the disk in this system is probably several orders of magnitude larger than the disks in CV.

Confirmation that the relative disk size $r_{\rm d}/r_{\rm i}$ is important may perhaps be found in binary protostars. Several cases are now known (see Matthieu, 1996) of relatively close binary protostars where at least one of the stars has a disk. The maximum size of such a disk can not be much larger than the tidal radius, something of the order of 1/3 of the orbital separation. The prediction is then that such disks do not produce well-collimated jets if $r_{\rm d} \lesssim 30 R_*$, i.e. if the orbital separation is less than about 0.5AU.

Acknowledgements This work was done in the Human Capitical and Mobility network 'Accretion in Close binaries' (CHRX-CT93-0329). I thank Rudi Stehle and Thierry Foglizzo for their comments on an early version of this text.

Table 1.2: Typical disk dimensions and minimum collimation angle for poloidal collimation, for different kinds of accretion disk systems.

	$r_{\rm i}$	$r_{\rm d}$	$\theta_{\rm min}$
protostars	0.01 AU	100 AU	0.01
LMXB	10 km	10^5km	0.01
AGN	1 AU	$> 10^4$AU	< 0.01
CV	10^4km	$2\,10^5$km	0.2
R Aqr	10^4km	$> 10^8$ km(?)	< 0.01

References

Bateman, G.: 1980, *MHD Instabilities*, Cambridge (Mass.): MIT press

Begelman, M.C., Blandford, R.D. and Rees, M.J.: 1984, *Rev. Mod. Phys.* **56**, 255

Begelman M.C. and Li Z.-Y., 1994, *Astrophys. J.,* **426**, 269

Bekenstein, J.D. and Oron, E.: 1978, *Phys. Rev D* **18**, 1809

Bisnovatyi-Kogan, G. and Ruzmaikin, A.A.: 1976, *Astrophys Sp. Sci.* **42**, 401

Blandford, R.D.: 1976, *Mon. Not. R. astron. Soc.,* **176**, 465

Blandford, R.D. and Payne, D.G.: 1982, *Mon. Not. R. astron. Soc.,* **199**, 883

Blandford, R.D.: 1993, in D. Burgarella, M. Livio and C. O'Dea, eds., *Astrophysical Jets*, Cambridge: Cambridge University Press, 15.

Brandenburg, A., Nordlund, Å., Stein, R.F. and Torkelsson, U.: 1995, *Astrophys. J.,* **446**, 741

Bridle, A.H. and Perley, R.A.: 1984, *Ann. Rev. Astron. Astrophys.,* **22**, 319

Burgarella, D. and Paresce, F.: 1992 *Astrophys. J.,* **389**, L29, errratum in **395**, 123

Camenzind, M.: 1987, *Astron. Astrophys.,* **184**, 341

Cao, X.-W. and Spruit H.C.: 1994, *Astron. Astrophys.,* **287**, 80

Choudhuri, A.R. and Königl, A.: 1986 *Astrophys. J.,* **310**, 96

Churazov, E., Sunyaev, R.A. and Gil'fanov, M., et al.: 1994, *Astrophys. J. Suppl.,* **92**, 381

Churazov, E., Gil'fanov, M., Sunyaev. R.A., et al.: 1993, *Astrophys. J.,* **407**, 752

Cisowski, S.M. and Hood, L.L.: 1991, in C. P.Sonnett, M.S. Giampapa, M.S. Matthews, eds., *The Sun in Time*, Tucson: Univ. of Arizona Press, p.761

Dougherty, S.M., Bode, M.F., LLoyd, H.M., Davis, R.J. and Eyres, S.P.: 1995 *Mon. Not. R. astron. Soc.,* **272**, 843

Drew, J.E. and Verbunt, F.: 1988, *Mon. Not. R. astron. Soc.,* **234**, 341

Eichler, D.: 1993, *Astrophys. J.,* **419**, 111

Foukal, P.V.: 1990, *Solar Astrophysics*, Wiley, New York, Chapter 12.3

Gallant, Y.A. and Arons J.: 1994, *Astrophys. J.,* **435**, 230

Galsgaard, K.: 1995, *J. Gephys. Res.* in press

Gil'fanov, M., Sunyaev, R.A., Churazov, E. et al.: 1991, *Pis'ma Astron. Zh.* **17**, 1059, translation in *Sov. Astron. Lett.* **17**, 437 (1992)

Goldreich, P. and Julian, W.H.: 1969 *Astrophys. J.,* **157**, 869

Goldreich, P. and Julian, W.H.: 1970 *Astrophys. J.,* **160**, 971

Hack, M. and La Dous, C., 1993, *Cataclysmic Variables and related objects*, NASA SP-507, Washington D.C.: US Printing Office

Hawley, J.F., Gammie, C.F. and Balbus, S.A.: 1995, *Astrophys. J.,* **440**, 742

Heinemann, M. and Olbert, S.: 1978, *J. Geophys. Res.* **83**, 2457

Heyvaerts, J. and Norman, C.A.: 1989, *Astrophys. J.,* **347**, 1055

Heyvaerts, J. and Norman, C.A.: 1996, preprint

Hjellming, R.M. and Rupen, M.P.: 1995 *Nature,* **375**, 464

Icke, V., Balick, B. and Frank, A.: 1992, *Astron. Astrophys.,* **253**, 224

Jeffrey, A. and Taniuti, T.: 1964, *Non-linear Wave propagation*, New York: Academic Press.

Königl, A.: 1989, *Astrophys. J.,* **342**, 208

Königl, A. and Ruden, S.P.: 1993, in *Protostars and Planets III*, eds. E.H. Levy,& J.I. Lunine, Tucson: Univerity of Arizona Press, 641

Levinson, A. and Blandford, R.D.: 1995, preprint 9506137, Los Alamos/Sissa e-print service

Lewin, W.H.G., van Paradijs, J. and van den Heuvel, E.P.J., eds.: 1995, *X-ray Binaries*, Cambridge Univ. Press, Cambridge

Li, Z., Chiueh, T. and Begelman, M.C.: 1992, *Astrophys. J.,* **394**, 459

Lichnérowicz, A.: 1967, *Relativistic hydrodynamics and magnetohydrodynamics*, New York: Benjamin.

Lovelace, R.V.E.: 1976 *Nature,* **262**, 649

Lovelace, R.V.E., Wang, J.C.L. and Sulkanen, M.E.: 1987, *Astrophys. J.,* **315**, 504

Lubow, S., Papaloizou, J.C.B. and Pringle, J.E: 1994, *Mon. Not. R. astron. Soc.,* **268**, 1010

Lubow, S. and Spruit, H.C: 1995, *Astrophys. J.,* **445**, 337

Mathieu, R.: 1996 in R.A.M.J. Wijers, C.A. Tout and J.E. Pringle (eds.) *Physical processes in Binaries*, Kluwer Dordrecht, (NATO ASI series).

Mestel, L.: 1968 *Mon. Not. R. astron. Soc.,* **138**, 359

Michel, F.C.: 1969 *Astrophys. J.,* **158**, 727

Michel, F.C.: 1973 *Astrophys. J.,* **180**, L133

Mirabel, I.F., Cordier, B., Paul and J., Lebrun, F.: 1992, *Nature,* **358**, 215

Mirabel, I.F. and Rodriguez, L.F.: 1994 *Nature,* **371**, 46

Nitta, S.-y.: 1994, *Publ. Astr. Soc. Japan,* **46**, 217

Okamoto, I.: 1975, *Mon. Not. R. astron. Soc.,* **173**, 357

Okamoto, I.: 1978: *Mon. Not. R. astron. Soc.,* **185**, 69

Okamoto, I.: 1992, *Mon. Not. R. astron. Soc.,* **254**, 192

Parker, E.N.: 1963, *Interplanetary Dynamical Processes*, New York: Wiley.

Parker, E.N.: 1979, *Cosmical Magnetic Fields: Their Origin and Activity*, Oxford: Clarendon, Ch. 9

Pitts, E. and Tayler R.J.: 1985, *Mon. Not. R. astron. Soc.,* **216**, 139

Plumpton, C. and Ferraro, V.C.A: 1966, *Introduction to Magneto-fluid dynamics*, Oxford: Clarendon.

Pudritz R.E. and Norman C.A.: 1986 *Astrophys. J.,* **301**, 571

Rees, M.J., Begelman, M.C., Blandford, R.D. and Phinney, E.S.: 1982, *Nature,* **295**, 17

Roberts, P.H.: 1967 *An Introduction to Magnetohydrodynamics*, London: Longmans, p.235

Sakurai, T.: 1985, *Astron. Astrophys.,* **152**, 121

Sakurai, T.: 1987, *Publ. Astr. Soc. Japan,* **39**, 821.

Sauty, C. and Tsinganos, K.: 1994, *Astron. Astrophys.,* **287**, 893

Schatzman, E.: 1962 *Ann. Astrophys.* **25**, 18

Spruit, H.C.: 1994, in *Cosmical Magnetism*, ed. D. Lynden-Bell, Dordrecht: Kluwer, p. 33

Spruit, H.C., Stehle R.and Papaloizou, J.C.B.: 1995, *Mon. Not. R. astron. Soc.,* **275**, 1223

Spruit, H.C., Foglizzo, T. and Stehle R.: 1996, *Astron. Astrophys.,* in preparation.

Stewart, R.T., Caswell, J.L., Haynes, R.F., Nelson, G.J.: 1993, *Mon. Not. R. astron. Soc.,* **261**, 593

Strom, R.G., van Paradijs, J., van der Klis, M.; 1989 *Nature,* **337**, 234

Suess, S.T., Nerney, S.F.: 1975, *Solar Phys.,* **40**, 487

Sunyaev, R.A., Kaniovskii, A.S., Efremov, V.V. et al.: 1991, *Pis'ma Astron. Zh.* **17**, 291, translation in *Sov. Astron. Lett.* **17**(2), 123 (1991)

Tayler, R.J.: 1980 *Mon. Not. R. astron. Soc.,* **191**, 151

Thorstensen, J.R., Ringwald, F.A., Wade, R.A., Schmidt, G.D., Norsworthy, J.E.: 1991, *Astron. J.,* **102**, 272.

Tomimatsu, A.: 1994, *Publ. Astr. Soc. Japan,* **46**, 123

van Ballegooijen, A.A.: 1989, in *Accretion Disks and Magnetic Fields in Astrophysics*, ed. G. Belvedere, Dordrecht: Kluwer, p.99

Weber, E.J., Davis, L.: 1967 *Astrophys. J.,* **148**, 217

Index